BOREAS An international journal of Quaternary research

Seasonal precipitation variability on Svalbard inferred from Holocene sedimentary leaf wax δ^2H

SOFIA E. KJELLMAN, ELIZABETH K. THOMAS, WESLEY R. FARNSWORTH, OWEN C. COWLING, LIS ALLAART, SKAFTI BRYNJÓLFSSON AND ANDERS SCHOMACKER

BOREAS

Kjellman, S. E., Thomas, E. K., Farnsworth, W. R., Cowling, O. C., Allaart, L., Brynjólfsson, S. & Schomacker, A. 2024 (July): Seasonal precipitation variability on Svalbard inferred from Holocene sedimentary leaf wax δ^2H. *Boreas*, Vol. 53, pp. 430–452. https://doi.org/10.1111/bor.12661. ISSN 0300-9483.

Svalbard spans large climate gradients, associated with atmospheric circulation patterns and variations in ocean heat content and sea ice cover. Future precipitation increases are projected to peak in the northeast and to mainly occur in winter, but uncertainties underscore the need for reconstructions of long-term spatial and temporal variations in precipitation amounts and seasonality. We use lipid biomarkers from four sedimentary lake records along a climatic gradient from western to northeastern Svalbard to reconstruct Holocene water cycle changes. We measured the leaf wax hydrogen isotopic composition of long-chain (terrestrial) and mid-chain (aquatic) *n*-alkanoic acids, reflecting δ^2H of precipitation (δ^2H_{precip}) and lake water (δ^2H_{lake}), respectively. δ^2H_{precip} values mainly reflect summer precipitation δ^2H and evapotranspiration, whereas δ^2H_{lake} values can reflect various precipitation seasonality due to varying lake hydrology. For one lake, we used the difference between δ^2H_{precip} and δ^2H_{lake} ($\varepsilon_{precip\text{-}lake}$) to infer summer evapotranspiration changes. Relatively ^2H-enriched δ^2H_{precip} values and higher $\varepsilon_{precip\text{-}lake}$ in the Early and Middle Holocene suggest warm summers with higher evapotranspiration, and/or more proximal summer moisture. After *c.* 6 cal. ka BP, ^2H-depleted δ^2H_{precip} values and lower $\varepsilon_{precip\text{-}lake}$ indicate summer cooling, less evapotranspiration, or more distally derived moisture. Early to Middle Holocene decrease in δ^2H_{lake} values in two northern Spitsbergen lakes reflects an increase in the proportion of winter relative to summer precipitation, associated with regional warming and increased moisture supply, which may be due to increased distal moisture supply and/or reduced sea ice cover. Our northern Svalbard δ^2H_{lake} records suggest great Late Holocene climate variability with periodic winter precipitation increases or decreases in summer precipitation inflow to the lakes. We find that Holocene summer precipitation δ^2H values mainly follow changes in summer insolation and temperature, whereas the seasonal distribution of precipitation is sensitive to catchment hydrology, regional ocean surface conditions, and moisture source changes.

Sofia E. Kjellman (sofia.e.kjellman@uit.no), Lis Allaart and Anders Schomacker, Department of Geosciences, UiT The Arctic University of Norway, P.O. Box 6050 Stakkevollan, NO-9037 Tromsø, Norway; Elizabeth K. Thomas and Owen C. Cowling, Department of Geology, University at Buffalo, State University of New York, 126 Cooke Hall, Buffalo, NY 14260, USA; Wesley R. Farnsworth, Institute of Earth Sciences, University of Iceland, Askja, Sturlugata 7, IS-102 Reykjavík, Iceland and Globe Institute, University of Copenhagen, Øster Voldgade 5-7, DK-1350 Copenhagen, Denmark; Skafti Brynjólfsson, Icelandic Institute of Natural History, Borgum við Norðurslóð, IS-600 Akureyri, Iceland; *Present address: Near Surface Land and Marine Geology, Geological Survey of Denmark and Greenland (GEUS) Universitetsbyen 81, DK-8000 Aarhus C, Denmark;* *received 10th July 2023, accepted 26th April 2024.*

The Svalbard archipelago is located on the primary pathway for atmospheric energy transport to the Arctic (Serreze *et al.* 2007). Over the last 50 years, annual precipitation on Svalbard have increased by 20–35% (Førland *et al.* 2020), and heavy precipitation events have become more intense and frequent (Hanssen-Bauer *et al.* 2019; Lapointe *et al.* 2023). Müller *et al.* (2022) attributed extreme winter precipitation events on Svalbard in the last four decades to declining sea ice cover in the Greenland Sea, providing a source of moisture. Regional models project an annual precipitation increase of around 65% from 1971–2000 to 2071–2100 (ensemble median, emission scenario 'business as usual'; Hanssen-Bauer *et al.* 2019). The increase is heterogenous in both time and space, being most pronounced in the winter months and with the largest increase in the northeast. These future projections are associated with large uncertainties due to limitations in the climate models and inadequate knowledge about the sensitivity of the climate system (Hanssen-Bauer *et al.* 2019).

Most of our understanding of past and present-day Arctic hydrological change is based on *in situ* and remote sensing observations, atmospheric reanalyses, and climate model hindcasts (e.g. Dufour *et al.* 2016; Førland *et al.* 2020; Wickström *et al.* 2020). We can improve our understanding of the mechanisms behind precipitation changes through palaeoclimate proxies, which allow reconstructions beyond the short and sparse instrumental records (e.g. Linderholm *et al.* 2018; Konecky *et al.* 2020). Water isotope proxies (i.e. $\delta^{18}O$ or δ^2H in ice-cores, diatom biogenic silica, chironomids, lacustrine carbonates, lipids etc.) are commonly used in palaeoclimate research, as they reflect multiple aspects of the water cycle, including temperature and moisture source changes (Masson-Delmotte *et al.* 2005; Cowling *et al.* 2021; Katrantsiotis *et al.* 2021), moisture balance (Anderson *et al.* 2007; Balascio *et al.* 2013) and precipitation seasonality (Thomas *et al.* 2020; Corcoran *et al.* 2021).

Many recent studies use the hydrogen isotopic composition of sedimentary leaf waxes (δ^2H_{wax}) to reconstruct

DOI 10.1111/bor.12661

the isotopic composition of Arctic precipitation in the past (e.g. Thomas *et al.* 2012, 2016, 2018, 2020; Wilkie 2012; Balascio *et al.* 2013; Keisling *et al.* 2017; Cowling *et al.* 2021; Daniels *et al.* 2021; Gorbey *et al.* 2021), including on Svalbard (Balascio *et al.* 2018; Kjellman *et al.* 2020). Leaf wax δ^2H values reflect the δ^2H values of the plant source water (lake or soil water, which are ultimately recharged by precipitation) with an offset (apparent fractionation, ε_{app}) due to climatic and/or plant physiological drivers (Sessions *et al.* 1999; Kahmen *et al.* 2013) such as biosynthetic fractionation (ε_{bio}; Sachse *et al.* 2012). The biosynthetic fractionation can differ between plant types (Daniels *et al.* 2017; Berke *et al.* 2019; Dion-Kirschner *et al.* 2020) but is relatively constant for specific leaf wax compounds (Sachse *et al.* 2012; McFarlin *et al.* 2019). The catchment-integrated ε_{app} values are likely similar for aquatic and terrestrial plant waxes (Thomas *et al.* 2020).

Studies of the modern relationship between δ^2H_{wax} and δ^2H of precipitation have demonstrated that there is a strong correlation between the two, with the leaf wax values being more ^2H-depleted than precipitation (Sachse *et al.* 2004, 2012; McFarlin *et al.* 2019). Yet, it is challenging to directly convert δ^2H_{wax} values to precipitation δ^2H values. The isotopic composition of meteoric water is influenced by changes in temperature, moisture source, precipitation amount and precipitation seasonality (Dansgaard 1964; Rozanski *et al.* 1993). Furthermore, the δ^2H values of the plant source water, and therefore the δ^2H_{wax} values, can be modulated by catchment-integrated processes (e.g. Sachse *et al.* 2012; Diefendorf & Freimuth 2017). Due to our incomplete understanding of the relative importance of processes influencing the isotopic composition of leaf waxes, δ^2H_{wax} values are typically used for qualitative rather than quantitative assessment of water cycle changes. The potential of using wax–water calibration is improving, but there are no calibration data sets from Svalbard. Calibration using global data might in fact artificially introduce more uncertainty than what is realistic, considering that the catchment-integrated uncertainties are likely smaller than the uncertainties of the global calibration data set (McFarlin *et al.* 2019), which contains large uncertainties due to large variability in catchment vegetation and climate. Therefore, it is advisable, if possible, to apply wax–water calibration using a data set representative of the local conditions.

Different aspects of the water cycle can be separated by using a dual-biomarker approach (Rach *et al.* 2017). This method assumes that we can trace the leaf waxes back to aquatic or terrestrial sources, and the environmental water pools used by the different organisms. Terrestrial plants use soil water as their source water, and the hydrogen isotopic composition of terrestrial leaf waxes therefore reflects growing season soil water δ^2H values, which might be influenced by evaporation (Kahmen *et al.* 2013). Aquatic plants use lake water as their moisture source, so that the hydrogen isotopic composition of aquatic leaf waxes reflects ice-free growing season lake water δ^2H values. The lake water δ^2H values can reflect different precipitation seasonality depending on the residence time of the lake (Cluett & Thomas 2020; Thomas *et al.* 2020).

Globally, studies have shown that aquatic plants primarily produce mid-chain waxes (Ficken *et al.* 2000; Aichner *et al.* 2010), whereas terrestrial plants produce high concentrations of long-chain waxes (Sachse *et al.* 2012; Diefendorf & Freimuth 2017). Similar observations have been made in the Arctic (e.g. Thomas *et al.* 2016, 2020; Kjellman *et al.* 2020), although some recent studies are challenging this conventional source attribution, as Arctic shrubs can produce large amounts of C_{22} and C_{24} *n*-alkanoic acids (Daniels *et al.* 2017; McFarlin *et al.* 2019; Dion-Kirschner *et al.* 2020). One key factor controlling the wax sources in Arctic lakes appears to be the relative abundance of aquatic bryophytes in the lake compared to the terrestrial contribution from the catchment (Hollister *et al.* 2022).

Here, we present Holocene leaf-wax derived records of the isotopic composition of precipitation (δ^2H_{precip}) and lake water (δ^2H_{lake}) from four lakes in the high-Arctic archipelago Svalbard. The aim of this study is to document how different parts of Svalbard have responded to past climate change, and more specifically to reconstruct Holocene variations in precipitation seasonality in time and space. We targeted lakes along a climatic gradient from the relatively warm, humid western Spitsbergen to the relatively cold, arid Nordaustlandet (Fig. 1). The lakes reflect different precipitation seasonality due to their different water residence times, and we regard the biomarkers from the lake sediment successions as archives of regional palaeoclimate. Further, we discuss our findings in relation to established terrestrial and marine palaeoenvironmental records as well as the glaciation history of Svalbard.

Regional setting

High-Arctic Svalbard (latitude 74–81°N, longitude 10–35°E) is one of the world's northernmost landmasses, but the archipelago experiences warmer, wetter and cloudier conditions than other areas at the same latitude (Eckerstorfer & Christiansen 2011). This is mainly due to the strong influence of the warm West Spitsbergen Current and associated northward atmospheric heat and moisture transport along the west coast of Spitsbergen (Skagseth *et al.* 2008; Walczowski & Piechura 2011; Fig. 1A). The interplay between warm Atlantic and cold Arctic ocean currents and atmospheric air masses, as well as pronounced topography, cause regional differences in climate, with milder conditions on the west coast and colder and drier climate in the central parts and in the northeast (Hisdal 1998).

Available climate data from Svalbard are limited, with meteorological stations concentrated on low-elevation coastal western Spitsbergen (Nordli

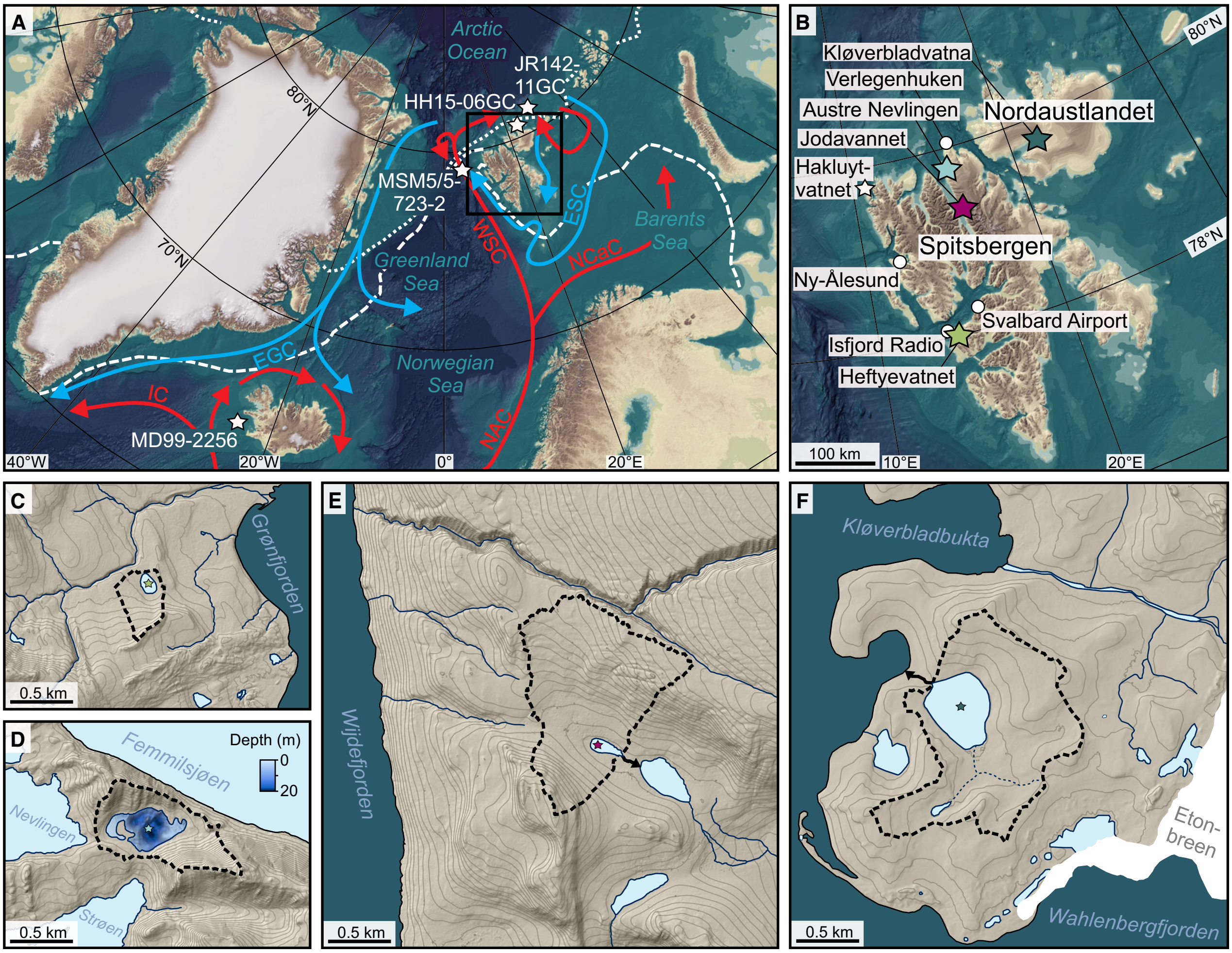

Fig. 1. A. Overview map of the North Atlantic region, with major ocean surface currents (warm currents in red, cold in blue; NAC = North Atlantic Current; NCaC = North Cape Current; WSC = West Spitsbergen Current; IC = Irminger Current; ESC = East Spitsbergen Current; EGC = East Greenland Current), median winter (white dashed line) and summer (white dotted line) sea-ice extent AD 1981–2010 (National Snow and Ice Data Center 2019), and locations of marine cores (white stars) MSM5/5-723-2 (Werner *et al.* 2016), HH15-06GC and JR142-11GC (Pieńkowski *et al.* 2021), and MD99-2256 (Jennings *et al.* 2015). B. Map of Svalbard, showing locations of lakes in this (coloured stars) and previous (white star; Balascio *et al.* 2018) studies and meteorological stations (white circles). Coring locations (stars) and lake catchments (black dashed lines) for Heftyevatnet (C), Austre Nevlingen (D), Jodavannet (E) and Kløverbladvatna (F). Black arrows mark outflow streams. Background maps in A–B from IBCAO (Jakobsson *et al.* 2012) and in C–F based on 5 × 5 m digital elevation models from the Norwegian Polar Institute (2014) with 10-m contour lines.

et al. 1996). The alpine topography of Spitsbergen has a strong orographic influence on precipitation. Snow accumulation is 40% higher on the east coast compared to the west coast, with the steepest east–west gradient in the south (Sand *et al.* 2003). There is also a south–north gradient, with the south receiving approximately twice as much precipitation as the north. This gradient is steepest in the central and eastern parts. Large local gradients also occur (Humlum 2002). For instance, precipitation amounts in Longyearbyen are approximately three times lower than along the west coast of Spitsbergen, less than 50 km away (Førland & Hanssen-Bauer 2003).

Modern precipitation isotopes have been measured at two sites on the west coast of Spitsbergen as part of the Global Network of Isotopes in Precipitation (GNIP; IAEA/WMO 2019). Monthly precipitation δ^2H and δ^{18}O values at Isfjord Radio (78.07°N, 13.63°E; 1961–1965, 1972–1975) and in Ny-Ålesund (78.92°N, 11.93°E; 1990–2016) do not exhibit a seasonal trend, whereas the deuterium excess (d-excess = $\delta^2H - 8 \times \delta^{18}O$; Dansgaard 1964) is over 6‰ higher during the winter months at both sites (IAEA/WMO 2019; Fig. 2). The values fall close to the Global Meteoric Water Line (GMWL, $\delta^2H = 8 \times \delta^{18}O + 10$; Craig 1961; Fig. 3). There are no precipitation isotope measurements from central and northeastern Svalbard, but stronger isotopic seasonality is expected due to the larger contrast between summer and winter climate farther from the open water along the west coast.

To explore regional differences in palaeo-precipitation trends, we targeted four lakes across Svalbard:

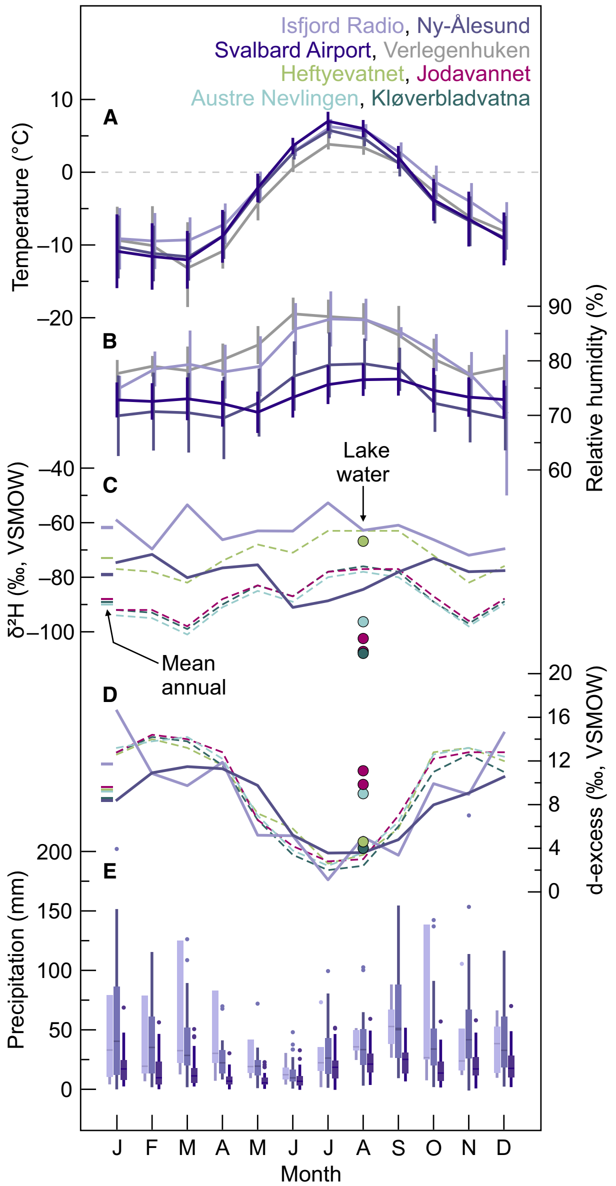

Fig. 2. Climate data from Svalbard Airport, Ny-Ålesund, Isfjord Radio and Verlegenhuken (for locations, see Fig. 1). A. Mean monthly air temperatures and B. Relative humidity between 1991 and 2020 (2011–2020 for Verlegenhuken). Vertical bars represent 1σ standard deviation. Amount-weighted monthly Global Network of Isotopes in Precipitation (GNIP; IAEA/WMO 2019). C. δ^2H and D. d-excess in precipitation (solid lines) from Isfjord Radio (1961–1965, 1972–1975) and Ny-Ålesund (1990–2016), estimated precipitation δ^2H values for all sites (dashed lines) calculated using the Online Isotopes in Precipitation Calculator (OIPC; Bowen *et al.* 2005; IAEA/WMO 2019; Bowen 2021), and August lake surface water values (measured 2018–2022; Fig. 3). E. Monthly accumulated precipitation, 1991–2020. For each box plot, the middle line displays the median precipitation, the box represents the 25 to 75% quartile range, whiskers are maximum and minimum values, and dots are outliers. Temperature and precipitation data were retrieved from MET Norway (2021). There were no precipitation data available for Verlegenhuken.

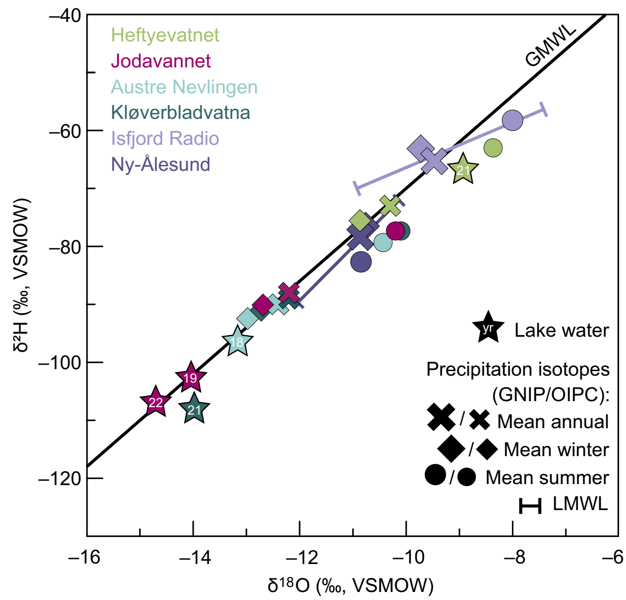

Fig. 3. Co-isotope plot with modern summer (August) lake water isotope values (numbers indicate year of sampling: 18 = 2018 etc.), amount-weighted mean annual, mean ice cover (October–June = winter) and mean ice-free season (July–September = summer) precipitation values from the Global Network of Isotopes in Precipitation (GNIP; IAEA/WMO 2019), and modelled precipitation values from the Online Isotopes in Precipitation Calculator (OIPC; Bowen *et al.* 2005; IAEA/WMO 2019; Bowen 2021). The data are plotted against the Global Meteoric Water Line (GMWL; $\delta^2H = 8 \times \delta^{18}O + 10$) and Local Meteoric Water Lines (LMWLs) for Isfjord Radio and Ny-Ålesund.

Heftyevatnet on the west coast of central Spitsbergen, Austre Nevlingen and Jodavannet on north-central Spitsbergen, and Kløverbladvatna on Nordaustlandet (Fig. 1B–F and Data S1). The four selected lakes are fed by catchment runoff, and do not currently receive glacial meltwater. The precipitation seasonality reflected in the lake and soil water is influenced by a range of factors, including the relative amount of winter and summer precipitation falling in the catchment, the lake water residence time, and the duration of ice cover on the lake (Thomas *et al.* 2020). No long-time series of lake ice phenology exist from Svalbard. On western Spitsbergen, the ice-free season at smaller lakes is from early July to early October (Kongressvatnet; Holm *et al.* 2012), and ice freeze-up at larger lakes starts later in October (Linnévatnet; Tuttle *et al.* 2022). In the cooler north-eastern part of Svalbard, the ice-free period is likely shorter, from July to September. Aquatic plants produce most of their waxes during the ice-free season, since primary production is controlled by light availability and temperature (Guo *et al.* 2013; Riis *et al.* 2014). Terrestrial leaf waxes are likely produced throughout the short

Arctic growing season (Shanahan *et al.* 2013; Daniels *et al.* 2017; Freimuth *et al.* 2017), which in most parts of Svalbard starts in mid-June to early July and ends in early September (Karlsen *et al.* 2014; ORNL DAAC 2018).

Material and methods

Seasonal lake water residence time calculations

To infer the precipitation seasonality reflected in the lake water, we estimated seasonal (ice-cover and ice-free season) residence times for the four lakes (Tables 1, S1). These calculated residence times are rough estimates, considering the poor constraints on precipitation amounts falling on northern and northeastern Svalbard. Svalbard Airport is located more than 100 km south of Austre Nevlingen and Jodavannet, and more than 200 km southwest of Kløverbladvatna, with mountains, ice caps, fjords, and sounds in between (Fig. 1B).

Modern lake water δ^2H analysis

To better constrain the precipitation seasonality reflected in lake water δ^2H values and to quantify the influence of evaporative enrichment, we collected surface water samples from the four lakes during field campaigns in August 2018, 2019, 2021 and 2022. The samples were collected from the shoreline in 4-mL glass vials with no headspace, sealed with Parafilm, and stored cold until analysis. For details on the analytical procedures, see Kjellman (2022). By comparing the lake water δ^2H values to regional precipitation δ^2H values we can assess the seasonality reflected in the lake water δ^2H values. Heftyevatnet is 14 km southeast of Isfjord Radio, whereas the other lakes are far away from the closest GNIP station. Precipitation δ^2H values at the lake sites were estimated using the Online Isotopes in Precipitation Calculator (OIPC; Bowen *et al.* 2005; IAEA/WMO 2019; Bowen 2021). The uncertainty in these interpolated values is considerable (in the order of 20–30‰) due to the lack of Arctic precipitation isotope data (Bowen & Revenaugh 2003). They might not capture local variability due to the coarse grid resolution, but they do provide the only available estimate. In Tromsø, northern Norway, Kjellman *et al.* (2022) found that the mean annual OIPC-modelled δ^2H value (−111‰) was 42‰ more depleted than the amount-weighted mean annual precipitation δ^2H value (−69‰) based on 2 years of precipitation sampling. In that case, the closest GNIP stations are located >150 km more inland and at higher elevations, suggesting that lake water δ^2H values might be better indicators of precipitation δ^2H values than OIPC-modelled values in areas far away from and in different settings to the closest GNIP stations. Since our lake water isotope measurements are actual observations, we weight them more heavily than the residence time calculations and the OIPC values when deciding on the seasonality interpretation.

Precipitation isotope seasonality simulations

To assess the sensitivity of precipitation δ^2H seasonality to different moisture sources, we used a one-dimensional Rayleigh distillation model after Fritz & Clark (1997) and Cluett *et al.* (2021). The model was forced by six scenarios of seasonal variations in the cooling of moisture from source to sink, at a monthly resolution. We tested two sources for the moisture arriving to Svalbard; a distal North Atlantic source using temperature and vapour δ^2H values from southwest Iceland (Steen-Larsen *et al.* 2015; Icelandic Met Office 2024), and a local Svalbard source using temperature and vapour δ^2H values from Ny-Ålesund (Leroy-Dos Santos *et al.* 2020; MET Norway 2021). For the sink temperatures, we ran the simulations for one sink on the west coast (Isfjord Radio) and one on northernmost Spitsbergen (Verlegenhuken; MET Norway 2021; Fig. 1). Additionally, we tested sink temperatures adjusted for high elevation, since the moisture must travel over ~1000-m-high mountains to reach northern Svalbard. We emphasize that this simple model only tests two different sources (comparing proximal and distal moisture) and two sinks (comparing western and northern Spitsbergen) based on available modern data, and does not necessarily show the complete range of possible precipitation isotope values. Details on the model simulations are given in the Supporting Information (Data S2 and Table S2).

Sediment cores

We present data from nine sediment cores collected from the four lakes between 2015 and 2019. Detailed

Table 1. Lake water residence times and percentage of water replaced during spring melt and throughout the ice-free season. For details on the calculations, see Table S1.

Lake	Maximum lake water depth (m)	Lake area (km^2)	Catchment area (km^2)	Spring melt residence time (months)	Ice-free season residence time (months)	% of lake volume replaced during spring melt	% of lake volume replaced during ice-free season
Heftyevatnet	6.5	0.015	0.15	2.1	15.4	48.7	19.4
Jodavannet	6.4	0.020	1.31	0.8	4.2	131.7	71.3
Austre Nevlingen	18	0.13	0.48	28.3	156.7	3.5	1.9
Kløverbladvatna	17.5	0.23	1.64	19.0	105.4	5.3	2.8

methodology and full core descriptions and lithostratigraphy are presented by Schomacker *et al.* (2019) (Kløverbladvatna), Kjellman *et al.* (2020) (Austre Nevlingen), Voldstad *et al.* (2020) (Jodavannet), Farnsworth *et al.* (2022) (Heftyevatnet), and in Fig. S1.

Composite core construction and age-depth modelling

Age-depth models based on radiocarbon ages have previously been presented by Schomacker *et al.* (2019), Kjellman *et al.* (2020), Voldstad *et al.* (2020) and Farnsworth *et al.* (2022). To improve the resolution for Heftyevatnet, we picked out and dated seven additional bryophyte samples (Table S3). We also present three new radiocarbon ages from a surface core from Jodavannet. For Kløverbladvatna, we combined ages from both cores into a composite age-depth model. With these additional constraints, we generated new age-depth models for Heftyevatnet, Jodavannet and Kløverbladvatna.

To generate one composite sedimentary record for each lake, we aligned the overlapping surface and piston cores in AnalySeries (v. 2.0.8; Paillard *et al.* 1996), using tie-points in the elemental data (Fig. S2). All proxy and chronological data were entered into Linked PaleoData (LiPD) files (McKay & Emile-Geay 2016), and age-depth models (Fig. S3) were generated in R (v. 4.1.3; R Core Team 2021) using Bacon (v. 2.5.7; Blaauw & Christen 2011) within the geoChronR package (v. 1.1.5; McKay *et al.* 2021). For each record, we set the upper depth (d.min) to the uppermost leaf wax sample depth and the lower depth (d.max) to the lowermost leaf wax or radiocarbon sample depth. For records where changes in lithology suggested changes in sedimentation rate, we added boundaries and adjusted the prior mean accumulation rates (bacon.acc.mean; Fig. S3). The rest of the settings were kept at the default values. One sample from Kløverbladvatna and one sample from Jodavannet that were used as age-constraints in the previously published models (Schomacker *et al.* 2019; Voldstad *et al.* 2020) appeared to be outliers (Fig. S3). All radiocarbon ages were (re)calibrated using the IntCal20 data set (Reimer *et al.* 2020) and are presented in calibrated years before present (cal. a BP; BP = 1950; Table S3). For Jodavannet, we used the age-depth model from Voldstad *et al.* (2020) to guide us during subsampling for leaf wax analysis, whereas the data are presented using the current age-depth model (Fig. S3). This affects the sample resolution at the end of the Early Holocene (higher resolution) and most of the Middle Holocene (lower resolution). The age ensembles were mapped to the leaf wax data, allowing us to present proxy data with age model uncertainty.

Lipid biomarker extraction and analysis

Biomarker analyses were performed in the University at Buffalo Organic and Stable Isotope Biogeochemistry Laboratory. Sediment samples (3–4 cm^3 for Heftyevatnet, Austre Nevlingen, and Kløverbladvatna, 6–8 cm^3 for Jodavannet) were collected based on estimated age (Heftyevatnet, Jodavannet, Kløverbladvatna) or depth (Austre Nevlingen), depending on the status of available chronological data at the time of sampling. Methods for leaf wax extraction, purification and *n*-alkanoic acid analysis followed previously published procedures (Thomas *et al.* 2012; Kjellman *et al.* 2020). The total lipid extract (TLE) was extracted from freeze-dried sediments using a Dionex 200 Accelerated Solvent Extractor with dichloromethane (DCM):methanol 9:1 (v/v). After adding $C_{20:1}$ *n*-alkanoic acid (Fisher Scientific, 4.2 μg) as an internal standard, the compounds in the TLE were separated into neutral and acid fractions using flash-column chromatography with aminopropyl silica gel solid phase, eluting neutral compounds with DCM:isopropanol 2:1 (v/v) and acids using 4% acetic acid in DCM. We methylated the acid fraction at 60 °C overnight using 5% anhydrous HCl in methanol with a known isotopic composition and cleaned the samples on silica gel columns, eluting the fatty acid methyl esters (FAMEs) in DCM.

FAME peak areas were quantified on a Thermo Scientific Trace 1310 gas chromatograph (GC) equipped with two flame ionization detectors (FIDs) operated in parallel, with AI1310 autosamplers and two split/splitless injectors. The inlets were held at 250 °C and operated in splitless mode for 45 s, after which split flow was turned on at 14 mL min^{-1}. After that, we held a constant column flow of 3.6 mL min^{-1} using hydrogen carrier gas. The oven was held at an initial temperature of 70 °C for 1 min, then ramped to 230 °C at 27 °C min^{-1}, followed by a final ramp to 315 °C at 6 °C min^{-1}, where we held for 10 min. Compounds were identified by retention time, using an added internal standard as a reference. We calculated FAME concentrations using external calibration curves determined for a C_{28} FAME standard and normalized the FAME masses to the dry mass of extracted sediment and the recovery of the internal standard.

Hydrogen isotope analyses of the FAMEs were conducted on a Thermo Scientific Delta V Plus isotope ratio mass spectrometer (IRMS) coupled via an Isolink II and Conflo IV to a Trace 1310 GC. We used the FAME concentrations to dilute and inject target amounts of compounds. The GC conditions and programs were the same as those used during FAME quantification, except that we used helium as the carrier gas at a flow rate of 1.5 mL min^{-1}. The H_3^+ factor was determined at the beginning of every sequence, ranging from 2.19±0.02 to 5.00±0.04 ppm nA^{-1} (Table S4). We ran samples in triplicate (or in duplicates or singles for small samples) along with FAME standards of known isotopic composition (A. Schimmelman, University of Indiana) to constrain drift (C_{18} and C_{24}) and linearity (C_{20} and C_{28}) and to normalize all δ^2H values to the Vienna Standard Mean Ocean Water (VSMOW) scale. We also corrected FAME δ^2H values for hydrogens added during methylation. To constrain the peak-size effects on the measured isotopic composition we injected the C_{20} and C_{28} FAME standards at a range of masses. We excluded peaks that were below a threshold (~2–4 Vs for each sequence) where the uncertainty of the linearity correction was too high. For samples that were between the standard constraints (i.e. with peak areas below the threshold but within the range of standard peak areas), we compared the triplicate (or duplicate) injections and kept sample peaks with similar δ^2H values. For sequences without clear linearity and small C_{20} and/or C_{30} peaks (about one-third of the Jodavannet and 80% of the Heftyevatnet samples), all C_{20} (Jodavannet and Heftyevatnet) and C_{30} (Heftyevatnet) injections were discarded. All isotope values are reported using standard δ notation in per mil (‰) relative to VSMOW:

$$\delta^2H(‰) = \left(\frac{R_{sample}}{R_{VSMOW}} - 1\right) \times 1000 \quad (1)$$

where R is the ratio between deuterium and hydrogen, $^2H/^1H$.

We calculated the total uncertainty of measured δ^2H values as the standard error of the mean (SEM), which equals the square root of the sum of the squares of total measurement uncertainty for each sample (drift and peak size corrections, replicate uncertainty of sample measurements, uncertainty in the δ^2H value of the methanol-derived hydrogens), divided by the square root of the number of measurements. The average SEM was 3.9‰ for Heftyevatnet, 2.7‰ for Jodavannet, 2.7‰ for Austre Nevlingen and 2.4‰ for Kløverbladvatna. C_{20}, C_{22} and C_{30} had higher average SEM (3.2–3.7‰) than C_{24}, C_{26} and C_{28} (2.6‰).

We calculated the average chain length (ACL) for C_{22} to C_{30} even chain lengths using Equation 2:

$$ACL_{22-30} = \frac{\sum(n \times C_n)}{\sum(C_n)} \quad (2)$$

where C_n is the μg g^{-1} dry sediment of each *n*-alkanoic acid with *n* carbon atoms. The carbon preference index (CPI) was calculated as:

$$CPI_{22-30} = 0.5 \times \left(\frac{\sum_{even}(C_{22}-C_{28})}{\sum_{odd}(C_{23}-C_{29})} + \frac{\sum_{even}(C_{24}-C_{30})}{\sum_{odd}(C_{23}-C_{29})}\right). \quad (3)$$

Leaf wax δ^2H to lake water and precipitation δ^2H conversion

We calculated lake water (δ^2H_{lake}) and precipitation (δ^2H_{precip}) δ^2H values from aquatic and terrestrial leaf wax δ^2H values using Equations 4 and 5:

$$\delta^2H_{lake} = \left(\frac{1000 + \delta^2H_{C_{22}}}{\frac{\varepsilon_{C_{22}-lake}}{1000} + 1}\right) - 1000 \quad (4)$$

$$\delta^2H_{precip} = \left(\frac{1000 + \delta^2H_{C_{28}}}{\frac{\varepsilon_{C_{28}-precip}}{1000} + 1} - 1000\right) \quad (5)$$

where $\delta^2H_{C_{22}}$ and $\delta^2H_{C_{28}}$ are the C_{22} and C_{28} leaf wax δ^2H values, and $\varepsilon_{C_{22}-lake}$ and $\varepsilon_{C_{28}-precip}$ are the apparent fractionation between lake water and C_{22} in surface sediments and summer precipitation and C_{28} in soil. We used apparent fractionation factors of −123±7‰ and −115±15‰ for $\varepsilon_{C_{22}-lake}$ and $\varepsilon_{C_{28}-precip}$, respectively. These apparent fractionation factors were determined using surface sediment and sediment trap C_{22} and soil C_{28} *n*-alkanoic acid δ^2H values (Hollister *et al.* 2022) and ice-free season lake water δ^2H and summer precipitation δ^2H values (Gorbey *et al.* 2022) from Baffin Island, Canada. We consider these calibration data to be the most representative for Svalbard since the sites have fairly similar climate (low-lying/coastal, cold, high-Arctic) and vegetation (terrestrial: graminoids, dwarf shrubs, moss mats; aquatic: dominated by submerged mosses). The total proxy uncertainty was calculated as the square root of the sum of the squares of the analytical uncertainty and the conversion uncertainty. The average total proxy uncertainty for the δ^2H_{lake} values was 7.9‰ for Heftyevatnet, 7.6‰ for Jodavannet, 7.8‰ for Austre Nevlingen and 7.5‰ for Kløverbladvatna, whereas the average total proxy uncertainty for the δ^2H_{precip} values was 15.3‰ for Heftyevatnet and 15.2‰ for Jodavannet, Austre Nevlingen, and Kløverbladvatna.

For Heftyevatnet, we calculated the isotopic difference between precipitation and lake water ($\varepsilon_{precip-lake}$) using Equation 6:

$$\varepsilon_{precip-lake} = \left(\frac{1000 + \delta^2H_{precip}}{1000 + \delta^2H_{lake}} - 1\right) \times 1000 \quad (6)$$

Depending on the lake hydrology, time series of this value can reflect changes in relative humidity (Rach *et al.* 2017) or precipitation seasonality (Thomas *et al.* 2020). We calculated the total uncertainty for $\varepsilon_{precip-lake}$ as the square root of the sum of the squares of the total uncertainties of δ^2H_{precip} and δ^2H_{lake} values. The average uncertainty for all lakes was 17.3‰.

Results

Lake water residence times and lake water δ^2H seasonality

Heftyevatnet (large catchment-to-lake ratio, Fig. 1C) has a median spring melt residence time of 2 months, meaning that approximately half of the lake water is flushed during spring melt and ~20% of lake water is replaced by summer precipitation during the ice-free season (Tables 1, S1). Modern lake water δ^2H at Heftyevatnet (−66.8±0.40‰ (±1σ)) is close to ice-free season precipitation δ^2H values at Isfjord Radio, and d-excess (4.6±0.6‰) is close to summer precipitation d-excess (Figs 2, 3). This suggests that most of the water in the lake is flushed by water with isotope values close to summer precipitation during the growing season, perhaps due to large inputs from active layer thaw (Gorbey *et al.* 2022) or that snow-melt input to this lake is minimal, due to 'snow-melt bypass', i.e. snow melting off the landscape before the lake becomes ice-free (MacDonald *et al.* 2017). The short residence time and lake water δ^2H value in line with modelled precipitation δ^2H values suggest that the lake water reflects summer precipitation δ^2H and experiences minimal evaporative enrichment (Fig. 3).

The residence time calculations indicate that the lake water in Jodavannet (large catchment-to-lake ratio; Fig. 1E) is flushed by spring melt in less than a month and that more than two-thirds of the lake water is replaced during the ice-free season (Tables 1, S1). Yet, modern lake water δ^2H values from Jodavannet (−102.5±0.02‰; −106.6±1.30‰) are more depleted than modelled winter precipitation δ^2H values and have d-excess (9.9±0.07‰; 11.1±1.80‰) close to modelled mean annual precipitation d-excess (Figs 2, 3). Modern lake water plotting close to the GMWL indicated that Jodavannet is not significantly influenced by evaporation (Fig. 3).

Austre Nevlingen (small catchment-to-lake ratio; Fig. 1D) has no distinct outflow and a median spring melt residence time of 28 months, suggesting that less than 4% of the lake volume is flushed by ^{2}H-depleted snow-melt each year (Tables 1, S1). The median ice-free season residence time is 157 months (13 years), suggesting that only ~2% of the lake water is replaced during the growing season. The modern lake water δ^2H value (−96.3±0.17‰) is close to modelled winter precipitation δ^2H values and d-excess (9.0±0.27‰) is close to mean annual precipitation d-excess, indicating minimal evaporative enrichment despite the long residence time (Figs 2, 3; Kjellman *et al.* 2020).

Kløverbladvatna (small catchment-to-lake ratio; Fig. 1F) has a median spring melt residence time of 19 months (Tables 1, S1), indicating that the exchange of water in the lake is slow. Only ~5% of the lake water is estimated to be replaced during the spring melt, and ~3% during the ice-free season. The modern lake water δ^2H value (−107.9±0.40‰) is more ^{2}H-depleted than modelled winter precipitation δ^2H values (Fig. 2) and falls slightly below the meteoric water line (d-excess = 4.0±0.6‰; Fig. 3), suggesting that Kløverbladvatna is dominated by winter precipitation inputs and is influenced by evaporative enrichment.

Sensitivity of precipitation δ^2H to moisture source changes

In addition to different seasonality, we tested the effect of varying source and sink conditions on the precipitation δ^2H values, using a Rayleigh distillation model. The sensitivity tests showed that the relatively most ^{2}H-enriched precipitation δ^2H values were achieved with a local (Ny-Ålesund) source to western Svalbard (Isfjord Radio), whereas the most ^{2}H-depleted precipitation δ^2H values were obtained with a distal (SW Iceland) source to northern Svalbard (Verlegenhuken), taking the height of the mountains into account (Fig. 4). However, these tests were only run for two theoretical moisture sources and sinks, based on available modern data (Steen-Larsen *et al.* 2015; Leroy-Dos Santos *et al.* 2020; MET Norway 2021; Icelandic Met Office 2024), and may therefore not cover the full range of precipitation δ^2H values that can be achieved. The temperatures and isotopic ranges have presumably varied in the past and over longer time scales, and there are other possible sources that could experience very different conditions. Moreover, in reality the precipitation falling at a given location will be a mix of moisture from various sources. One important observation is that the effect of a shifting moisture source on precipitation δ^2H is greater than the range of modelled seasonal variability.

Leaf wax-derived δ^2H_{precip} and δ^2H_{lake} values

Details on leaf wax concentrations and chain-length distributions are given in Data S3. For most parts of the four leaf wax records, the leaf wax homologues can be separated into two groups, with the mid-chain waxes (C_{20}, C_{22} and C_{24}) and long-chain waxes (C_{26}, C_{28} and C_{30}) displaying similar isotope values within each group, but different values when comparing the two (Figs S4–S7). We therefore infer them to originate from two different plant sources: aquatic and terrestrial plants (see details on source attribution in the Discussion). For simplicity, we hereafter focus on the δ^2H_{precip} and δ^2H_{lake} values calculated from δ^2H of C_{22} and C_{28} *n*-alkanoic acids, originating from aquatic and terrestrial leaf waxes, respectively.

Generally, δ^2H_{lake} showed more ^{2}H-depleted values than δ^2H_{precip}, especially in Austre Nevlingen and Jodavannet (Figs 5, S5A, S6A). In contrast, Kløverbladvatna had relatively ^{2}H-depleted δ^2H_{precip} compared to δ^2H_{lake} values until *c.* 3.1 cal. ka BP, and thereafter δ^2H values that varied by less than 20‰ among all homologues (Fig. S7A). Heftyevatnet displayed more similar δ^2H_{lake} and δ^2H_{precip} values, with $\varepsilon_{precip\text{-}lake}$ always lower than 30‰ (Figs 5, S4D). Austre Nevlingen and Jodavannet also showed larger amplitude δ^2H_{lake} variability than Kløverbladvatna and Heftyevatnet (Fig. 5).

In Heftyevatnet, the δ^2H_{precip} and δ^2H_{lake} values co-varied for most of the record (Fig. 5). From 12.1 to

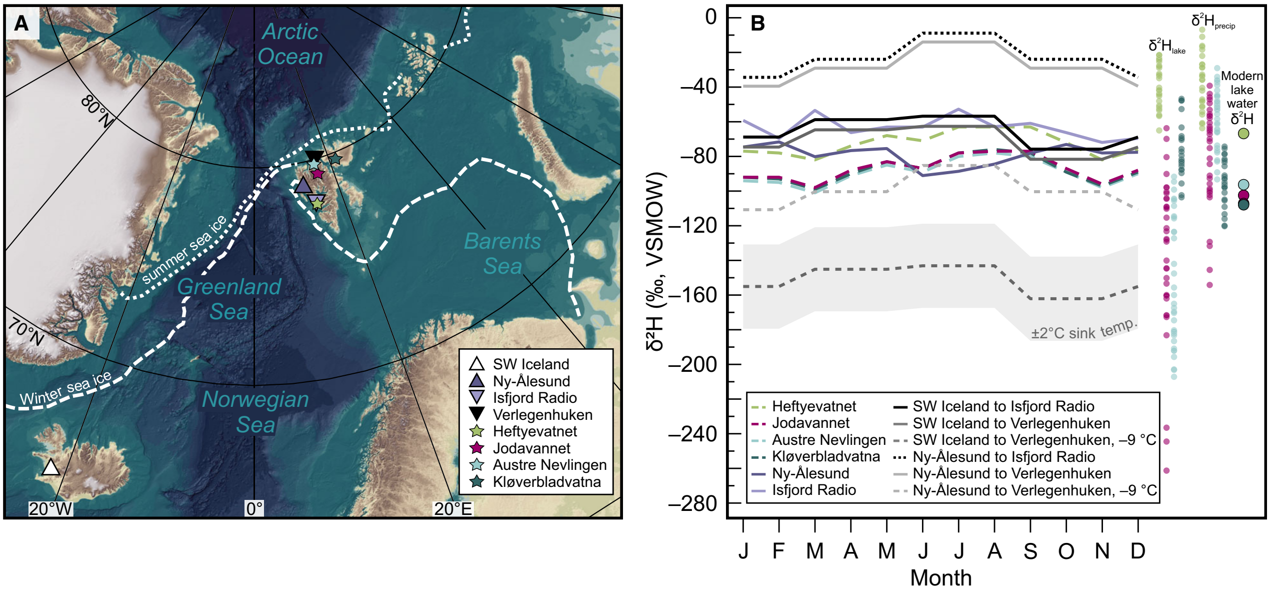

Fig. 4. Simulated seasonal precipitation isotope patterns on Svalbard for locally and distally sourced moisture. A. Moisture sources and sinks used in the simulations (triangles) and the four study sites (stars). Sea-ice extent AD 1981–2010 from National Snow and Ice Data Center (2019) and background map from IBCAO (Jakobsson *et al.* 2012). B. Simulated monthly precipitation δ^2H from six Rayleigh distillation simulations (grey; Table S2), precipitation δ^2H for all sites (Heftyevatnet, Jodavannet, Austre Nevlingen, and Kløverbladvatna) calculated using the Online Isotopes in Precipitation Calculator (OIPC; Bowen *et al.* 2005; IAEA/WMO 2019; Bowen 2021), and measured precipitation δ^2H from Isfjord Radio (1961–1965, 1972–1975) and Ny-Ålesund (1990–2016; IAEA/WMO 2019). The grey envelope for the most ^{2}H-depleted scenario (source: SW Iceland, sink: Verlegenhuken −9 °C) shows precipitation δ^2H values for a sink temperature change of ±2 °C. The impact of temperature change on other sensitivity tests is similar. Leaf wax-derived δ^2H_{lake} and δ^2H_{precip} values and measured summer lake surface water δ^2H values are plotted for comparison.

10.9 cal. ka BP, the δ^2H_{precip} values fluctuated between −40 and −16‰, whereas the δ^2H_{lake} values decreased from −22 to −29‰ and continued to decrease until 7.2 cal. ka BP (−48‰). From 11.0 to 8.0 cal. ka BP, the δ^2H_{precip} values increased to −11‰, after which they fluctuated between −29 and −7‰ until 6.2 cal. ka BP. After one ^{2}H-enriched value at 6.2 cal. ka BP (−7‰ for δ^2H_{precip} and −24‰ for δ^2H_{lake}), both the δ^2H_{precip} and δ^2H_{lake} values showed a distinct drop, to −51 and −57‰, respectively. After 5.4 cal. ka BP, the δ^2H_{precip} values stayed between −64 and −36‰, whereas the δ^2H_{lake} values fluctuated between −65 and −24‰.

Jodavannet δ^2H_{precip} and δ^2H_{lake} values displayed a similar trend for most of the Holocene, but the δ^2H_{lake} values had larger amplitude changes (Fig. 5). In the Early Holocene both chain lengths experienced a rapid increase (from −154 to −39‰ for δ^2H_{precip}, and from −160 to −70‰ for δ^2H_{lake}) until *c.* 10.5 cal. ka BP. From 10.5 to 4.9 cal. ka BP, the δ^2H_{precip} values decreased to −71‰, and the δ^2H_{lake} values to −183‰. After 4.9 cal. ka BP, the δ^2H_{precip} values continued decreasing with a similar trend, except for one more ^{2}H-depleted value (−129‰) at 4.3 cal. ka BP. The δ^2H_{lake} values experienced larger amplitude variability, fluctuating between −261 and −98‰. For the latest 0.7 cal. ka BP, δ^2H_{precip} and δ^2H_{lake} displayed similar values (between −121 and −91‰).

Austre Nevlingen displayed relatively ^{2}H-depleted δ^2H_{precip} values in the Early Holocene, with an increasing trend until 9.5 cal. ka BP, after which the δ^2H_{precip} values fluctuated between −34 and −53‰, with a slightly decreasing trend (Fig. 5). In the Early Holocene, the δ^2H_{lake} values showed an opposite trend to the δ^2H_{precip} values, decreasing from −92 to −203‰ between 11.2 and 8.5 cal. ka BP. From 8.5 to 6 cal. ka BP, the δ^2H_{lake} values remained mostly ^{2}H-depleted between −207 and −115‰ (Fig. 5). After 6 cal. ka BP the δ^2H_{lake} values display larger amplitude variability, fluctuating between −203 and −95‰.

The Kløverbladvatna δ^2H record started 5.2 cal. ka BP, with relatively ^{2}H-depleted δ^2H_{precip} values in the Middle Holocene (Fig. 5). The δ^2H_{precip} values decreased from −98‰ at 5.2 cal. ka BP to −120‰ at 4.5 cal. ka BP, before increasing to −91‰ at 3.6 cal. ka BP. During the same period (5.2–3.6 cal. ka BP) the δ^2H_{lake} values decreased from −48 to −76‰ (Fig. 5). After 3.6 cal. ka BP, δ^2H_{precip} and δ^2H_{lake} values followed a similar trend (Fig. 5), increasing until 1.9 cal. ka BP (to −75 and −77‰, respectively), decreasing from 1.9 to 0.9 cal. ka BP (to −92 and −104‰, respectively), and increasing again for the last 0.9 cal. ka BP (to −74 and −71‰, respectively).

Discussion

Modern isotope hydrology on Svalbard

Interpretation of leaf wax-derived δ^2H values is aided by an understanding of modern precipitation isotope

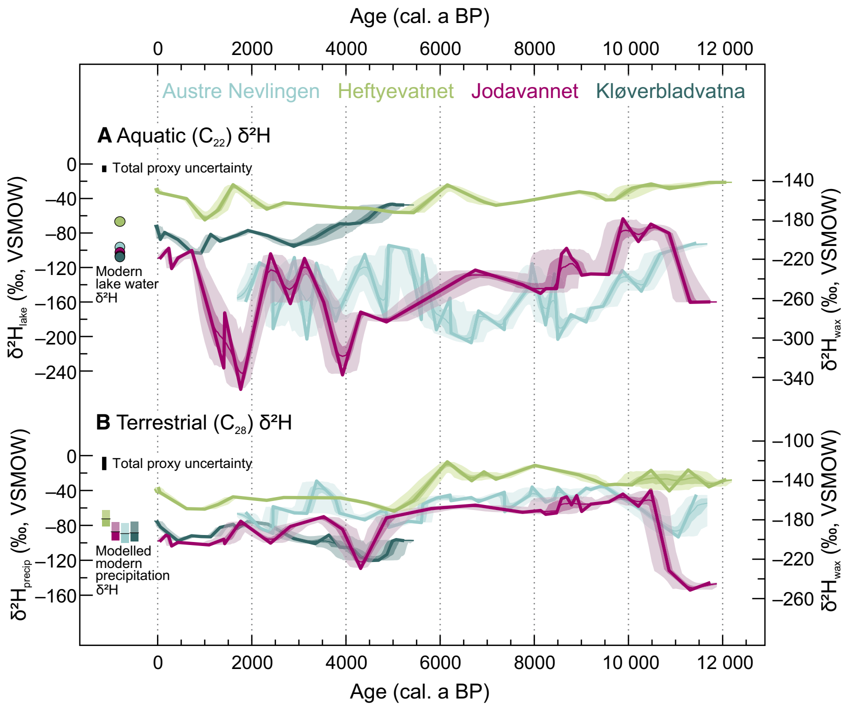

Fig. 5. Leaf wax δ^{2}H values (right axis) and leaf wax δ^{2}H converted to lake water or precipitation δ^{2}H values (left axis) for aquatic (C_{22}) (A) and terrestrial (C_{28}) (B) plant *n*-alkanoic acids from Heftyevatnet, Jodavannet, Austre Nevlingen, and Kløverbladvatna, Svalbard. Bold line: measured values plotted on the median age of each sample; fine line: median value of all age model iterations; light and dark shading: 1σ and 2σ age model uncertainty, respectively. The vertical black bars represent the total proxy uncertainty and include analytical and conversion uncertainties. Modern summer lake water δ^{2}H values (circles) and modelled precipitation δ^{2}H values (bars; representing ranges between weighted mean annual (black line) and maximum and minimum monthly precipitation) from the Online Isotopes in Precipitation Calculator (OIPC; Bowen *et al.* 2005; IAEA/WMO 2019; Bowen 2021) are plotted for comparison.

variability and by observation-based constraints on lake, soil, surface sediment, and plant water δ^{2}H values (e.g. Daniels *et al.* 2017; Berke *et al.* 2019; McFarlin *et al.* 2019; Cluett & Thomas 2020; Dion-Kirschner *et al.* 2020; Hollister *et al.* 2022). On Svalbard, there are few such constraints and only two locations with precipitation isotope observations, both on the windward west coast, meaning that we rely heavily on modelled precipitation isotope values, which have large uncertainties in this region (Bowen & Revenaugh 2003) and due to coarse spatial resolution likely do not fully reflect the strong distillation that occurs due to the complex topography.

In the Arctic, there is usually a strong correlation between the isotopic composition of precipitation and local temperature (Dansgaard 1964). However, no robust relationship exists between mean monthly precipitation δ^{2}H values and air temperature measured at Isfjord Radio or Ny-Ålesund (Fig. 2). We interpret this as caused by seasonally variable moisture sources, a process that explains a similar lack of seasonal precipitation δ^{2}H variability on western Greenland (Cluett *et al.* 2021). Northern Spitsbergen and Nordaustlandet are more frequently influenced by Arctic air masses, and North Atlantic moisture gets strongly distilled when travelling over the mountains, explaining more pronounced precipitation and lake water δ^{2}H seasonality on northern Svalbard than on the west coast.

To explore the factors influencing modern lake water seasonality, we use lake water δ^{2}H values. Comparing our summer lake water data to the observed and OIPC-modelled values, the Heftyevatnet ice-free season lake water δ^{2}H value is close to summer precipitation δ^{2}H values from Isfjord Radio (14 km northwest of the lake; Figs 1–3). The rest of the lakes are far from the sites with measured precipitation isotopes. The Austre Nevlingen lake water δ^{2}H value is close to the OIPC-modelled winter values, whereas Jodavannet and Kløverbladvatna are too ^{2}H-depleted to be explained by any of the modelled values (winter, summer, or a mix of seasons). In addition, despite their proximity, Jodavannet sits at a higher elevation than Austre Nevlingen, with a higher-elevation catchment, which would make precipitation isotopes ^{2}H-depleted relative to modelled values.

In addition to seasonality, the conditions at the moisture source and sink locations, including temperature and sea ice cover, and the moisture transport history have a large impact on precipitation isotope values on Svalbard. Müller *et al.* (2022) linked intensified winter precipitation over Svalbard since the 1980s to reduced sea-ice extent in the Greenland Sea, highlighting the role of sea ice east of Greenland in the southerly moisture transport to Svalbard in winter. In contrast, during times of extensive sea ice in the Greenland Sea, moisture from lower latitudes is transported over the sea ice (i.e. lifted and cooled), resulting in increased precipitation over the sea ice and reduced evaporation of ocean surface water. Our Rayleigh distillation sensitivity tests (Fig. 4) show that precipitation from a local (Ny-Ålesund) moisture source passing the mountains reaches δ^2H sink values that closely resemble the modern lake water samples from Austre Nevlingen, Jodavannet, and Kløverbladvatna. Because of the low spatial resolution of the OIPC model, the effect of distillation over the mountains is not fully taken into account in the OIPC-modelled precipitation δ^2H values (Fig. 4). The most ^{2}H-depleted precipitation δ^2H values are reached when distal (North Atlantic) moisture travels over the mountains to northern Svalbard in winter. If, like other Arctic regions, Svalbard mainly receives moisture evaporated from oceanic sources in winter and with a larger contribution of moisture evapotranspired from terrestrial sources in summer (Vázquez *et al.* 2016; Singh *et al.* 2017; Nusbaumer *et al.* 2019; Bonne *et al.* 2020; Cluett *et al.* 2021; Harrington *et al.* 2021), then it is likely that the northern Svalbard sites experience a stronger seasonal precipitation isotope gradient (i.e. ^{2}H-depleted winter precipitation derived from distal North Atlantic sources, and ^{2}H-enriched summer precipitation derived from local moisture sources) than is modelled by the OIPC. In addition, due to the large isotope differences between different sources, changes in moisture source contributions in the past could result in large changes in precipitation isotope values, as has been demonstrated at other Arctic sites (Thomas *et al.* 2018, 2023; Broadman *et al.* 2020).

Furthermore, a process that is likely important on Svalbard is snow-melt bypass (MacDonald *et al.* 2017). Satellite imagery suggests that large portions of the modern landscape become snow-free before the lake ice melts. During years with a shorter lake-ice season, more of the ^{2}H-depleted winter precipitation is likely to enter the lake. Furthermore, snow can be redistributed by the wind. Variable influence of these factors has implications for our leaf wax δ^2H interpretations.

Combining information from modern precipitation isotope observations, seasonal lake water residence time calculations, modern summer lake water isotopic composition, and Rayleigh distillation sensitivity testing suggests that the water in the different lakes reflects different seasonal signals today: Heftyevatnet is summer-biased, whereas Austre Nevlingen, Kløverbladvatna, and likely also Jodavannet, reflect mean annual to winter-biased precipitation. The simulated monthly precipitation δ^2H values also emphasize the influence of moisture source variability on precipitation δ^2H.

Leaf wax sources and precipitation isotope seasonality in Svalbard lake sediment records

Sources of mid- and long-chain n-alkanoic acids. – To interpret leaf wax-derived δ^2H records in terms of seasonal precipitation changes, we need to (i) identify the plant source of each leaf wax homologue, and (ii) determine the dominating seasonality of water used by the plants when they synthesize their waxes. Our Svalbard leaf wax homologues can be separated into two groups based on their δ^2H values (Figs S4–S7), which most likely reflect that they come from two different plant sources. There are almost no vascular aquatic plants on Svalbard, but aquatic bryophytes are abundant in Austre Nevlingen and Jodavannet, and produce abundant mid-chain waxes (Kjellman *et al.* 2020). Modern terrestrial plants from Svalbard (*Luzula confusa* and *Salix polaris*) have higher C_{28} relative to C_{22} concentration than aquatic bryophytes (Kjellman *et al.* 2020). We therefore interpret long-chain *n*-alkanoic acids to be derived from terrestrial plants and mid-chain *n*-alkanoic acids to be derived from aquatic plants, in accordance with previous studies (e.g. Ficken *et al.* 2000; Sachse *et al.* 2012; Wilkie *et al.* 2013; Daniels *et al.* 2017; Kjellman *et al.* 2020; Thomas *et al.* 2020; Hollister *et al.* 2022).

One possible exception to the two-sources interpretation (mid-chain waxes predominantly being produced by aquatic plants and long-chain waxes by terrestrial plants) is the Kløverbladvatna record, where there is no clear separation between long- and mid-chain waxes after 3.6 cal. ka BP (Fig. S7). We provide two possible explanations for this: (i) the waxes come from two different sources before 3.6 cal. ka BP and the same source after 3.6 cal. ka BP, or (ii) the waxes are derived from two sources, with similar δ^2H values after 3.6 cal. ka BP reflecting minimal evaporation. Balascio *et al.* (2018) interpreted similar δ^2H values and wax distributions similar to modern aquatic mosses to indicate that all waxes after *c.* 5 cal. ka BP in Hakluytvatnet, Amsterdamøya, northwestern Svalbard (Figs 1, 6D) were derived from aquatic plants, and therefore interpreted all chain lengths in that part of the record to reflect lake water δ^2H values. Similarly, in Kløverbladvatna, chain-length distributions change at 3.6 cal. ka BP (Fig. S7C). Before 3.6 cal. ka BP, C_{28} was the most abundant chain length, followed by C_{26} and C_{24}. After 3.6 cal. ka BP, C_{24} to C_{28} were still the dominating chain lengths, but with C_{24} being most abundant. We do not see a change in lithology at 3.6 cal. ka BP (Fig. S1D), and bryophytes and other aquatic plants are not abundant in this lake or its sedimentary record. It is possible that terrestrial plants were more dominant before 3.6 cal. ka BP, as suggested by the relatively higher C_{28} concentration, but based on our limited knowledge about *n*-alkanoic acid chain-length distribution of plants on Svalbard, and specifically in the Kløverbladvatna catchment, we cannot confirm a shift to higher aquatic production in

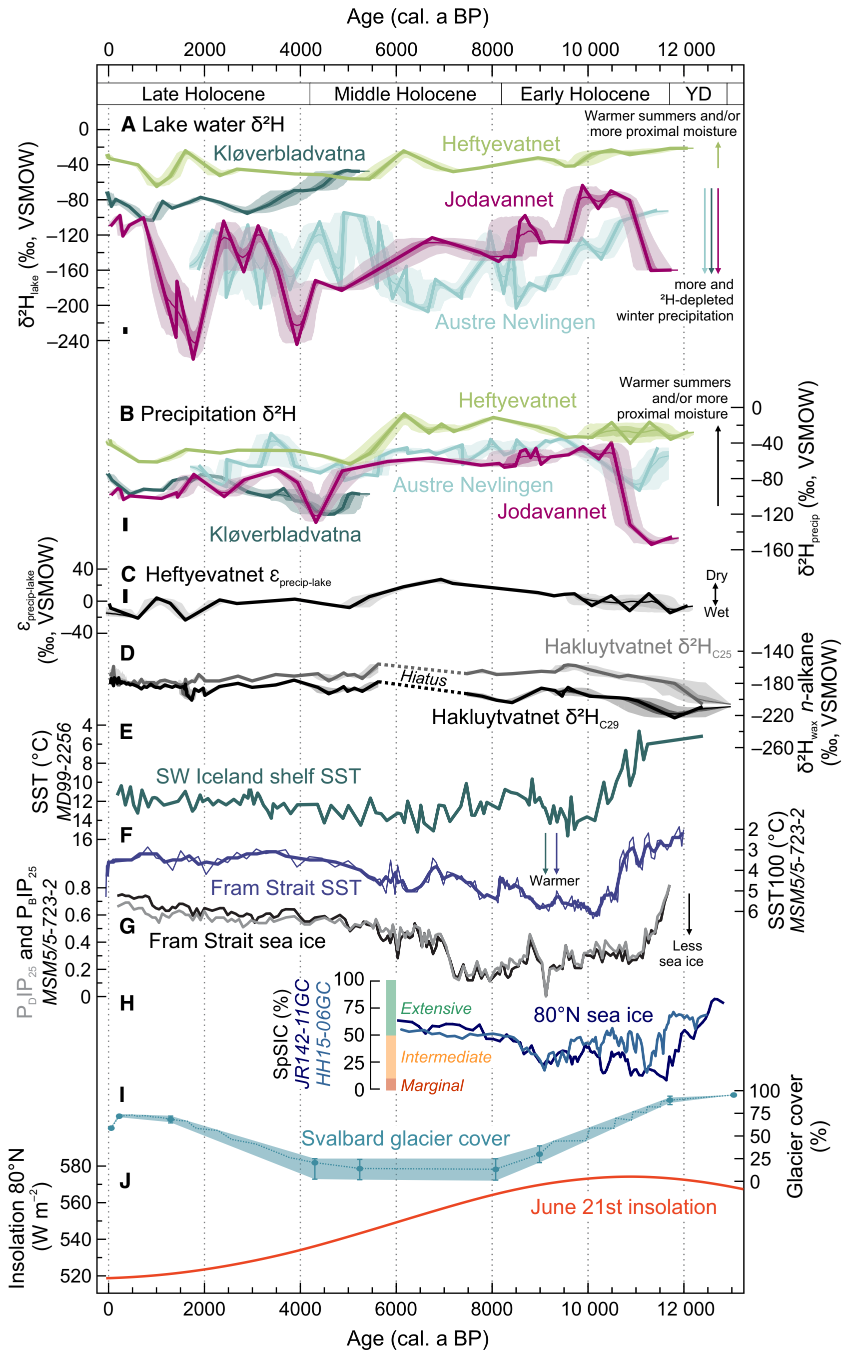

Fig. 6. Svalbard leaf wax-derived (*n*-alkanoic acid) hydrogen isotope data for lake water (C_{22}) and precipitation (C_{28}) from Heftyevatnet, Jodavannet, Austre Nevlingen, and Kløverbladvatna, compared to regional Holocene climate records. For locations, see Fig. 1. A. Lake water δ^2H. B. Precipitation δ^2H. C. Calculated isotopic difference between precipitation and lake water δ^2H ($\varepsilon_{precip-lake}$) for Heftyevatnet, inferred to reflect summer evapotranspiration. D. Lake Hakluytvatnet leaf wax δ^2H for C_{25} and C_{29} *n*-alkanes (Balascio *et al.* 2018). δ^2H_{C25} is interpreted to reflect δ^2H_{lake} values and δ^2H_{C29} to reflect δ^2H_{precip} values until *c.* 7.5 cal. ka BP. After *c.* 5 cal. ka BP, both records are interpreted to reflect δ^2H_{lake} values. E. Southwest Iceland Shelf sea-surface temperature (SST) estimates from planktic foraminiferal assemblages (Jennings *et al.* 2015). F. Eastern Fram Strait subsurface temperature based on planktic foraminiferal fauna assemblages (fine line; Werner *et al.* 2016), including 3-point running means (bold line; Husum & Hald 2012). G. Eastern Fram Strait spring sea-ice proxies P_BIP_{25} and P_DIP_{25} (based on brassicasterol and dinosterol, respectively; Werner *et al.* 2016). H. Biomarker-based spring sea-ice concentrations (SpSIC) from north of Nordaustlandet (Pieńkowski *et al.* 2021) with sea-ice categories sensu Köseoğlu *et al.* (2018). I. Estimated percentage of glacier cover across Svalbard (Farnsworth *et al.* 2020; modified from Fjeldskaar *et al.* 2018). J. June 21st insolation at 80°N (Laskar *et al.* 2004). Lines and shading in A–D are shown as in Fig. 5, and the black bars on the left in A–C represent total proxy uncertainty. Note that the *y*-axes in E–F are inverted.

the Late Holocene. Another possibility is that the dominant species producing C_{22} and C_{28} *n*-alkanoic acids are different in Kløverbladvatna compared to the other lakes, since the Kløverbladvatna catchment is dominated by mosses and lichen. The dominant wax producers could have changed at 3.6 cal. ka BP, thus causing the observed change in distributions and isotope values. Without more detailed information on the leaf wax sources, it is difficult to reach a single, simple interpretation. Because the catchment today is dominated by terrestrial plants with minimal aquatic plants, and aquatic plants are not abundant in the sedimentary record, we only interpret the C_{28} δ^2H values at Kløverbladvatna as a terrestrial record throughout the past 5.2 cal. ka BP, and do not interpret C_{22} δ^2H values, although further investigations into wax sources will be useful for this interpretation.

Seasonality of terrestrial leaf wax δ^2H. – Terrestrial leaf wax δ^2H values are often interpreted to reflect summer precipitation δ^2H values, based on the assumption that the soil water used by terrestrial plants when producing their waxes is mainly recharged by summer precipitation, which is supported by observations of summer-biased soil and/or xylem water isotopes (Cooper *et al*. 1991; Throckmorton *et al*. 2016; Daniels *et al*. 2017; Lamhonwah *et al*. 2017). This is likely true in most Arctic cases, especially in areas where the active layer becomes saturated towards the end of the preceding ice-free season and/or the winter precipitation stored as snow melts rapidly in early summer when the active layer is still frozen (Woo *et al*. 2008). However, this is complicated by the fact that snow patches and puddles of melted snow in some Arctic locations remain in the landscape for much of the growing season. Throughout summer, when the active layer of the permafrost thaws, some of this winter precipitation can percolate into the soil. In a study from a region in West Greenland that receives low summer precipitation amounts, meteoric water values estimated based on measurements on xylem water (assumed not to be isotopically fractionated from soil water) suggested that terrestrial plants utilize a mix of snow-melt and summer precipitation (Bush *et al*. 2017). Furthermore, in eastern Siberia, Sugimoto *et al*. (2003) observed more depleted soil water δ^{18}O values during a dry compared to a wet summer, suggesting that the amount of summer precipitation is important for whether the soil water in summer incorporates winter precipitation.

Some parts of Svalbard, in particular the Wijdefjorden region (including the Jodavannet and Austre Nevlingen catchments), receive very little precipitation in the summer months (Vikhamar-Schuler *et al*. 2019). If the active layer is not saturated at the end of summer, it might be partly recharged by winter precipitation during the snow-melt season. Soil moisture measurements in Ringhorndalen (~2 km from Jodavannet) between May and July 2017 showed that the main moisture source for terrestrial plants that summer was snow-melt early in the season rather than summer precipitation (Eidesen *et al*. 2018). The west coast of Svalbard receives more summer precipitation than the Wijdefjorden region (Vikhamar-Schuler *et al*. 2019), which saturates the active layer.

We do not have direct evidence for the seasonality of the soil water in our lake catchments, but based on the available data, we hypothesize that the δ^2H_{precip} values from all lakes are summer-biased, but propose that Jodavannet, Austre Nevlingen, and Kløverbladvatna δ^2H_{precip} values might incorporate some winter precipitation as well, due to more winter-biased soil water. This, and/or more Rayleigh distillation during moisture transport over mountain ranges to these northeastern lakes, can explain why these three lakes show ^{2}H-depleted δ^2H_{precip} values compared to Heftyevatnet (Fig. 6B). In addition to reflecting precipitation δ^2H values, terrestrial plant waxes can also be ^{2}H-enriched by evapotranspiration of soil and leaf water (e.g. Kahmen *et al*. 2013). More arid summer conditions in inner Wijdefjorden causing more evapotranspiration in the Jodavannet catchment than at Austre Nevlingen can explain the relatively ^{2}H-enriched δ^2H_{precip} values in Jodavannet compared to Austre Nevlingen, despite the proximity between the lakes.

Seasonality of aquatic leaf wax δ^2H. – Aquatic plants use lake water when producing their waxes, and therefore reflect the δ^2H value of the lake water during the growing season (e.g. Huang *et al*. 2004; Thomas *et al*. 2020). If the lake is flushed by spring melt (i.e. winter precipitation) and flushed again by summer precipitation and/or summer-biased groundwater, the lake water δ^2H values will be winter-biased during a brief period in the beginning of the ice-free season but biased towards summer precipitation δ^2H values for most of the growing season (Thomas *et al*. 2020; Gorbey *et al*. 2022). This is the case for Heftyevatnet, which we interpret to have summer-biased δ^2H_{lake} values. On the other hand, if the lake has a long residence time and/or does not receive enough runoff from summer precipitation, the lake water δ^2H values during the growing season can be closer to mean annual precipitation δ^2H values. A third option is to interpret δ^2H_{lake} values to be biased towards winter precipitation δ^2H (e.g. Katrantsiotis *et al*. 2021). Winter-biased lake water during the growing season can be the result of a higher proportion of the annual precipitation falling as snow, and late snow-melt (Jonsson *et al*. 2009; Kjellman *et al*. 2022).

Although Jodavannet has a large catchment-to-lake ratio and a short residence time, which would suggest the lake should be recharged by summer precipitation, it has lake water δ^2H values similar to Austre Nevlingen and Kløverbladvatna (i.e. mean annual to winter precipitation). There are several possible mechanisms that could explain why Jodavannet does not reflect summer precipitation despite its short residence time: (i) Due to its small volume and large catchment, Jodavannet is sensitive to short-term changes in seasonality, with the relative amounts of winter and summer precipitation modulating the lake water δ^2H values. (ii) Regional aridity and a relatively low proportion of summer precipitation likely cause summer precipitation to evaporate before it reaches the lake. (iii) Groundwater, likely at least partially recharged by winter precipitation in this region, might be an important source of water to the lake as the active layer thaws (Gorbey *et al*. 2022). Based on these observations, we interpret Austre Nevlingen and Jodavannet δ^2H_{lake} values to reflect mean annual or winter precipitation δ^2H changes.

Since the δ^2H_{lake} ranges in Jodavannet and Austre Nevlingen are greater than what can be explained by local precipitation, we infer both these lakes to be close to an isotopic threshold: we interpret the high-amplitude changes throughout the Holocene to indicate that these lakes shift between reflecting summer, mean annual, and winter precipitation δ^2H values. Large δ^2H_{lake} shifts suggest changing sensitivity of the lake basin to the seasonal distribution of precipitation (Kjellman *et al*. 2020). Some possible mechanisms explaining this change in sensitivity are variable duration of lake-ice cover, changes in the degree of snow-melt bypass, lake level changes, and varying degrees of summer evapotranspiration, affecting both the proportion of winter and summer precipitation that enters the lake and the lake water residence time.

The distinct δ^2H_{lake} changes could also be explained by a change in the source of the C_{22} *n*-alkanoic acids, which, if the plant source has different ε_{app}, would result in a different δ^2H_{lake} value without any change in the lake water δ^2H value. Both the Austre Nevlingen and Jodavannet sequences contain interbedded bryophytes, which may indicate that some samples were more dominated by bryophyte-derived waxes than others. However, the ^2H-depleted or ^2H-enriched values do not correspond with moss-dominated samples, nor do the bryophyte-rich samples contain major changes in the relative chain-length concentrations. The Late Holocene part of the Jodavannet record shows lower ACL (Fig. S5C), but for both relatively ^2H-enriched and ^2H-depleted samples.

Another recently proposed mechanism affecting the isotopic composition of mid-chain waxes derived from aquatic plant wax biomarkers is shifting lake methane cycling. McFarlin *et al*. (2023) introduce symbiosis between aquatic mosses and methanotrophic bacteria as a source to strongly ^2H-depleted δ^2H values in Greenland lakes, arguing that during some time periods, this methane-derived hydrogen overprints the lake water δ^2H signal.

We acknowledge that these processes or other mechanisms might help explain the data, but based on our current knowledge we choose to interpret large δ^2H_{lake} shifts to reflect lake or catchment processes that control the proportion of winter and summer precipitation entering the lake and/or the lake water residence time, rather than *n*-alkanoic acid source changes or shifts in lake methane dynamics.

Kløverbladvatna is located farthest east, where we lack good constraints on modern precipitation sources and isotopic composition, as well as on leaf wax sources. Since aquatic plants are neither abundant in the modern lake nor in the sedimentary record, and the lake water isotopes are influenced by evaporative enrichment, we do not interpret Kløverbladvatna in terms of aquatic leaf wax δ^2H values. For a summary of the interpretative framework for the seasonality reflected in each of the lake records, see Table S5.

Interpreting $\varepsilon_{precip\text{-}lake}$

The isotopic difference between the δ^2H of precipitation and lake water ($\varepsilon_{precip\text{-}lake}$) can be used to infer changes in summer evapotranspiration from sites meeting the following criteria: (i) the isotopic composition of the soil and lake water reflects the same precipitation seasonality, and (ii) the lake water does not experience evaporative enrichment, whereas the terrestrial plant source water does (Kahmen *et al*. 2013; Rach *et al*. 2017; Thomas *et al*. 2020). We have explained that Heftyevatnet fulfils these criteria, and therefore use $\varepsilon_{precip\text{-}lake}$ to reconstruct summer evaporative ^2H-enrichment of terrestrial plant source water.

Regional variability in Holocene precipitation isotope seasonality across Svalbard

Early Holocene: 11.7–8.2 cal. ka BP. – Distinct increases in δ^2H_{precip} and δ^2H_{lake} values in Jodavannet at the start of the Early Holocene likely reflect a shift from ^2H-depleted glacially derived source water to source water reflecting precipitation δ^2H values, also marked by the transition from glacial fine sand to silty gyttja (Figs 6A, B, S1B; Voldstad *et al*. 2020). After 10.5 cal. ka BP, the δ^2H_{precip} values stayed ^2H-enriched and relatively stable for the remainder of the Early Holocene. In Austre Nevlingen, increasing δ^2H_{precip} values from 11.0 to 9.6 cal. ka BP (Fig. 6B) suggest warming summer conditions with enhanced evaporative enrichment and/or a more proximal moisture source for growing season precipitation on northeastern Spitsbergen (Fig. 4).

Decreasing Austre Nevlingen δ^2H_{lake} values until 8.5 cal. ka BP (Fig. 6A) suggest an increasing proportion of ^2H-depleted winter precipitation and/or an increase in moisture transport from distal, North Atlantic sources contributing to the δ^2H_{lake} values. Kjellman *et al*. (2020) proposed that the very ^2H-depleted values in Austre Nevlingen reflected greater local winter evaporation due to reduced sea ice cover. Higher sea-surface temperatures in the North Atlantic during the same period (Jennings *et al.* 2015; Fig. 6E) suggest that increased evaporation and contribution from this distal moisture source may also have occurred at that time, similar to observations in recent decades linking increased winter precipitation on Svalbard to reduced Greenland Sea sea ice cover (Müller *et al.* 2022). In our Rayleigh distillation model, we tested the effect of distal vs. local moisture sources, showing that ^{2}H-depleted values can indeed be caused by an increase in the contribution of distal (North Atlantic) sources to Svalbard (Fig. 4).

For most of the Jodavannet record, δ^2H_{lake} follows δ^2H_{precip} (Fig. 5B), suggesting that both chain lengths are influenced by summer precipitation, although δ^2H_{lake} is also strongly affected by winter precipitation, as indicated by the more ^{2}H-depleted δ^2H_{lake} values. A stronger winter signal (i.e. more ^{2}H-depleted values) recorded in both Austre Nevlingen and Jodavannet suggests that this signal reflects climate variability, perhaps greater distal ocean surface evaporation resulting in increased winter precipitation amounts, rather than a change in individual lake dynamics. We cannot say whether this winter trend was consistent across Svalbard, as our δ^2H_{lake} record from the west coast (Heftyevatnet) reflects summer precipitation changes.

Heftyevatnet δ^2H_{precip} and δ^2H_{lake} values remained relatively stable throughout the Early Holocene (Fig. 6A, B), indicating stable summer conditions. Slightly increasing δ^2H_{precip} trend and higher $\varepsilon_{precip\text{-}lake}$ after 9.3 cal. ka BP (Fig. 6B, C) suggest higher summer evapotranspiration. Our Rayleigh distillation sensitivity tests suggest that the variability in the Heftyevatnet record could be due to changes in moisture sources in addition to changes in local temperature, and that local summer moisture sources were important on both western and northern Svalbard (Fig. 4).

Warmer summer conditions and more evaporation from ice-free seas during the Early Holocene agree with both terrestrial and marine environmental reconstructions. The onset of the Early Holocene was characterized by warm regional conditions and significant changes in ocean circulation, sea-ice extent, and glacier activity. The June solstice isolation at 80°N peaked around 11 cal. ka BP (Laskar *et al.* 2004; Fig. 6J), and warmer-than-present temperatures were recorded by alkenones in lakes on northwestern Spitsbergen *c.* 10 cal. ka BP (van der Bilt *et al.* 2019). Warmer Early Holocene conditions have also been shown by the presence of strongly thermophilous vascular plants in a *sed*aDNA record from Jodavannet (Voldstad *et al.* 2020). Balascio *et al.* (2018) interpreted increasing δ^2H values for C_{25} to C_{29} *n*-alkanes in Hakluytvatnet from 12.8 to 9.5 cal. ka BP to reflect insolation-driven warming and greater influence of mild sub-polar air masses. Furthermore, there was a substantial reduction in glacier cover on Svalbard in the Early Holocene (e.g. Svendsen & Mangerud 1997; Hald *et al.* 2004; Fjeldskaar *et al.* 2018; Farnsworth *et al.* 2020; Fig. 6I). However, despite various lines of evidence suggesting peak Holocene warmth, widespread glacier re-advances have been constrained to the Early Holocene (e.g. Lønne 2005; Farnsworth *et al.* 2018).

In the eastern Fram Strait, subsurface temperatures increased by 4 °C between 12 and 10.2 cal. ka BP (Werner *et al.* 2016; Fig. 6F), and shallow waters around Svalbard experienced temperatures 2–6 °C warmer than present between 11 and 9.2 cal. ka BP (Mangerud & Svendsen 2018). These changes have been interpreted to be a response to the high summer insolation and increased meridional Atlantic heat flux (Hald *et al.* 2007; Werner *et al.* 2016; Mangerud & Svendsen 2018). The pronounced inflow of warm Atlantic Water (AW) caused a reduction in sea ice cover in the eastern Fram Strait (Werner *et al.* 2016; Fig. 6G), as well as in many Svalbard fjord systems (Hald *et al.* 2004; Forwick & Vorren 2009; Bartels *et al.* 2017, 2018; Allaart *et al.* 2020). Although seasonal sea ice persisted in the northern Barents Sea throughout the warm Early Holocene, there were only intermediate concentrations (10–50%) until *c.* 9.1 cal. ka BP, followed by an increase towards predominantly extensive (>50%) sea ice by *c.* 8.3 cal. ka BP (Pieńkowski *et al.* 2021; Fig. 6H).

The decreasing Early Holocene sea-ice concentrations coincided with the decreasing δ^2H_{lake} values in Austre Nevlingen, suggesting that sea ice is a key driving force behind increased winter precipitation amounts on northern Spitsbergen (Kjellman *et al.* 2020). Another possible mechanism explaining the increased proportion of ^{2}H-depleted precipitation is increased moisture transport from distal, North Atlantic sources, likely during the autumn and winter (Fig. 4). Røthe *et al.* (2018) suggested higher winter precipitation amounts on northern Spitsbergen between 10.2 and 7 cal. ka BP, inferred from high frequency of ‘snow-melt layers’ (i.e. silty inorganic and graded sediment layers indicating rapid input of minerogenic material) in Vårfluesjøen. It is unclear whether this increase in winter precipitation on northern Svalbard was significant enough to locally outpace glacier ice mass loss caused by the high summer temperatures.

Middle Holocene: 8.2–4.2 cal. ka BP. – Austre Nevlingen δ^2H_{lake} values continued to be ^{2}H-depleted until *c.* 6 cal. ka BP (Fig. 6A), suggesting continued high winter precipitation amounts, associated with continuously low sea-ice extent in the Fram Strait (with increasing sea-ice extent from *c.* 7 cal. ka BP; Werner *et al.* 2016; Fig. 6G). Another possible mechanism explaining the ^{2}H-depleted δ^2H_{lake} values is high contribution of precipitation from distal sources (Fig. 4). As the temporal resolution for Jodavannet in the Middle Holocene is low (up to 1000 years between samples), we are not able to discuss this part of the record in detail, although the δ^2H_{lake} values are lower at 4.2 cal. ka BP than during the Early Holocene, suggesting greater influence of winter precipitation and/or more distally derived moisture.

Relatively stable δ^2H_{precip} values in Austre Nevlingen and Jodavannet and stable δ^2H_{precip} and δ^2H_{lake} values in Heftyevatnet until *c*. 6 cal. ka BP indicate stable summer conditions (Fig. 6A, B). Continuously high $\varepsilon_{precip\text{-}lake}$ at Heftyevatnet (Fig. 6C) indicates relatively higher summer evapotranspiration, likely due to dry summers on western Spitsbergen. Similar dry Middle Holocene summer conditions have been inferred from different proxies throughout Svalbard. At Hakluytvatnet, a hiatus in the sedimentary record from *c*. 7.5 to 5 cal. ka BP is interpreted to reflect non-deposition due to dry conditions and complete desiccation of the lake (Balascio *et al*. 2018; Gjerde *et al*. 2018; Fig. 6D). Warm and dry Middle Holocene conditions on northern Spitsbergen have also been suggested by Voldstad *et al*. (2020), based on the appearance of *Dryas* in the Jodavannet *sed*aDNA record.

After *c*. 6 cal. ka BP, lower $\varepsilon_{precip\text{-}lake}$ in Heftyevatnet and more ^2H-depleted δ^2H_{precip} values in all four lakes suggest that summer precipitation became ^2H-depleted due to cooler local temperatures or more distal moisture sources (Fig. 4), with less evaporative enrichment. Once again, this corroborates other evidence: sedimentation began again at Hakluytvatnet after 5 cal. ka BP, indicating wetter summers (Balascio *et al*. 2018; Fig. 6D). The widespread occurrence of the thermophilous mollusc *Mytilus edulis* indicates that Svalbard sea-surface temperatures were ~4 °C warmer than present between 8.2 and 6 cal. ka BP. After *c*. 6.2 cal. ka BP, the frequency of *Mytilus edulis* declined, and it disappeared from northern and eastern Svalbard by 5.7 cal. ka BP. This is interpreted as being due to declining sea-surface temperatures following the Holocene Thermal Maximum (Mangerud & Svendsen 2018). A similar trend is seen in the eastern Fram Strait, where sea-subsurface temperatures remained higher than at present (up to 5 °C) until *c*. 5 cal. ka BP (Werner *et al*. 2016).

Proglacial lake sediment records are characterized by reduced or absent minerogenic sedimentation in the Middle Holocene, indicating that glaciers were absent or much smaller than at present both on northern Spitsbergen (e.g. Røthe *et al*. 2015, 2018; Allaart *et al*. 2021) and western Spitsbergen (e.g. Svendsen & Mangerud 1997). The Holocene glacier minimum on Svalbard occurred between 8 and 6 cal. ka BP, with glaciers presumably covering ~25% of the land area in the north and east (Farnsworth *et al*. 2020; Fig. 6I). Surviving glaciers in the northeast could partly be explained by higher winter precipitation amounts, as suggested by the Austre Nevlingen δ^2H_{lake} record.

Late Holocene: 4.2–0 cal. ka BP. – The relatively stable or slight ^2H-depletion of summer precipitation continued on northern Spitsbergen in the Late Holocene, with relatively stable or slightly decreasing δ^2H_{precip} trends in Austre Nevlingen, Jodavannet, and Kløverbladvatna (Fig. 6B). Stable δ^2H_{precip} and δ^2H_{lake} values and low $\varepsilon_{precip\text{-}lake}$ in Heftyevatnet (Fig. 6A–C) suggested stable summer conditions and minimal evaporative enrichment of terrestrial plant source water on the west coast. Kløverbladvatna δ^2H_{precip} values increased by ~40‰ from 4.5 to 2 cal. ka BP and were in step with Jodavannet and Heftyevatnet δ^2H_{precip} values thereafter. All three records become slightly ^2H-depleted *c*. 1.5 to 0.5 cal. ka BP and slightly ^2H-enriched after 0.5 cal. ka BP. This strong similarity among δ^2H_{precip} records across Svalbard suggests similar summer precipitation sources and temperature during the Late Holocene.

Large fluctuations in the Austre Nevlingen and Jodavannet δ^2H_{lake} records, and strong differences between these records despite their proximity, indicate that the lakes reach a climate threshold and/or changes in the lake hydrology, altering the seasonality of precipitation, which is in turn reflected in the lake water. More variable δ^2H_{lake} values in Austre Nevlingen from 6 cal. ka BP into the Late Holocene was previously interpreted to reflect greater climate variability and that the lake recorded different precipitation seasonality (Kjellman *et al*. 2020). In the Late Holocene, the Jodavannet δ^2H_{lake} is decoupled from δ^2H_{precip}, indicating a stronger influence of winter precipitation and/or changing moisture sources causing ^2H-depletion. Concurrent changes in Jodavannet and Austre Nevlingen (e.g. decreasing δ^2H_{lake} values at the Middle to Late Holocene transition) could suggest the same climate forcing, whereas asynchronous changes (after *c*. 3.3 cal. ka BP) might be a result of changes in lake hydrology. Jodavannet, which has the largest catchment-to-lake area ratio, may be the most sensitive to changes in catchment and runoff dynamics that influence δ^2H_{lake} values. Indeed, Jodavannet contains the most ^2H-depleted and highly variable δ^2H_{lake} values during the Late Holocene. Together, these two lake records indicate a variable climate and/or changing moisture sources during the Late Holocene, which caused lake catchments to experience changes in winter runoff and in turn caused lake water isotope values to change dramatically on short time scales. Such mechanisms, caused by regional-scale climate changes, would impact Jodavannet and Austre Nevlingen to different degrees, due to their different catchment areas and volumes. Another possible factor causing more ^2H-depleted values in the Jodavannet record could be a Late Holocene increase in graminoids (having a larger ε_{bio} than shrubs, herbs and forbs; Sachse *et al*. 2012), as shown by Voldstad *et al*. (2020). However, this plant community change cannot explain the entire ^2H-depletion.

Drawing specific conclusions about the mechanisms causing the prominent variability in our δ^2H_{lake} records during the Late Holocene is not possible with currently available information, but we discuss them in relation to existing records from Svalbard. The Jodavannet lithology (Fig. S1B) and a distinct shift in the *sed*aDNA *c*. 4.3 cal. ka BP (Voldstad *et al*. 2020) are interpreted to reflect the onset of Neoglacial cooling. The neoglacial cooling is well documented on Svalbard, with lower temperatures inferred from plant macrofossils (Birks 1991), alkenones (van der Bilt *et al*. 2018), permafrost aggradation (Humlum 2005), snowline lowering (Miller *et al*. 2017), and glacier re-advances (e.g. Werner 1993; Svendsen & Mangerud 1997; van der Bilt *et al*. 2015; Røthe *et al*. 2015; Farnsworth *et al*. 2020; Allaart *et al*. 2021; Fig. 6I). The Neoglacial was generally characterized by decreasing insolation (Laskar *et al*. 2004; Fig. 6J), weakened AW advection, lower sea-surface temperatures and extended sea ice cover in the Fram Strait (e.g. Müller *et al*. 2012; Werner *et al*. 2013, 2016; Fig. 6F, G) and the Svalbard fjords (e.g. Forwick & Vorren 2009; Bartels *et al*. 2018).

Low sea-surface temperatures and extended sea ice cover likely inhibited local evaporation and reduced winter precipitation amounts on Svalbard. However, Müller *et al*. (2012) proposed that a temporarily strengthened West Spitsbergen Current and/or atmospheric circulation changes caused northward retreat of the sea-ice edge in the Fram Strait on several occasions during the Late Holocene, and that this triggered glacier advances on western Spitsbergen (Svendsen & Mangerud 1997). This is supported by abrupt increases in sea-surface temperature south of Svalbard *c*. 2.2 and 1.7 cal. ka BP (Sarnthein *et al*. 2003). Furthermore, Røthe *et al*. (2015) suggested that the (close to) maximum extent of Karlbreen on northwestern Spitsbergen from 1.7 to 1.5 cal. ka BP could be explained by open water conditions west of Spitsbergen (Müller *et al*. 2012). This coincided with ^{2}H-depleted δ^2H_{lake} values in Jodavannet (Fig. 6A), suggesting higher winter precipitation amounts on north-central Spitsbergen too, likely in combination with more distal (North Atlantic) moisture sources (Fig. 4). Increasing winter precipitation amounts have also been suggested to drive Little Ice Age (LIA, AD 1250–1920) glacier re-advances (D'Andrea *et al*. 2012; Arppe *et al*. 2017) but are not evident in our data.

Conclusions

We present leaf wax-derived Holocene δ^2H_{precip} and δ^2H_{lake} values from four lakes on Svalbard. In our records, we interpret δ^2H_{precip} values to mainly reflect summer precipitation δ^2H values and evapotranspiration, whereas δ^2H_{lake} values to reflect different seasonality depending on the residence time of the lake. The main findings are:

- Similar Holocene δ^2H_{precip} trends for all study sites suggest similar summer climate forcing across Svalbard. The Early and Middle Holocene summers were characterized by warmer, drier conditions and/or a more proximal moisture source, followed by a trend towards cooler conditions or more distally derived moisture from *c*. 6 cal. ka BP. Less ^{2}H-depleted δ^2H_{precip} values in Heftyevatnet reflect proximity to the North Atlantic, whereas the more ^{2}H-depleted δ^2H_{precip} values in Jodavannet, Austre Nevlingen, and Kløverbladvatna reflect more Rayleigh distillation during moisture transport over the mountains and/or incorporation of some winter precipitation due to more winter-biased soil water.
- In the Early Holocene, regional warming and increased moisture availability due to enhanced evaporation from ice-free seas and greater distal (North Atlantic) moisture contribution resulted in higher winter precipitation amounts and more ^{2}H-depleted δ^2H_{lake} values on northern Spitsbergen. The winter precipitation likely stayed high until the Middle Holocene, after which surface waters around Svalbard cooled and the sea ice cover increased, limiting the available moisture. During the Late Holocene, our northern Spitsbergen δ^2H_{lake} records suggest that periods of increased winter precipitation and great climate variability occurred. Additionally, asynchronous δ^2H_{lake} changes between the lakes indicate that changes in lake hydrology affected the seasonality reflected in the lake water δ^2H values.
- The precipitation seasonality reflected in the δ^2H_{lake} values may vary through time and space due to catchment processes that might be controlled by climate change. The δ^2H_{precip} seasonality might vary spatially depending on the seasonality of the precipitation recharging the active layer. To strengthen future palaeo-precipitation proxy studies on Svalbard, we need better constraints on modern precipitation sources and isotopic composition, soil and lake water recharge and evaporation, and site-specific leaf wax sources.

Acknowledgements. – This research was supported by grants from the Nansen Foundation to AS, The Arctic Research and Studies program of the Ministries for Foreign Affairs of Norway and Iceland (2017-ARS-79772) to AS, The Research Council of Norway (269984/E10) to AS, The Carlsberg Foundation (CF14-0756) to AS, Svalbard Environmental Protection Fund (16/35, 17/101, and 20/36) to AS, SEK and WRF, Olle Engkvists Stiftelse (204-0129) to AS and SEK, Helge Axe:son Johnsons Stiftelse to SEK, and National Science Foundation (EAR-IF 1652274) to EKT. We thank Sveinn Brynjólfsson, Sara Mollie Cohen, Lena Håkansson, Ólafur Ingólfsson, Marc Macias-Fauria and Michael Retelle for participating in fieldwork during lake sediment coring, and Michael Retelle and Tina Dahl for lake water sampling. We thank Katie Lovell for sample processing and are grateful to Nick McKay for LiPD troubleshooting and debugging. The anonymous reviewers are thanked for constructive comments that improved the manuscript. The authors declare that they have no known competing financial interests or personal relationships that could have appeared to influence the work reported in this paper.

Author contributions. – SEK: conceptualization, investigation, visualization, writing – original draft, project administration, funding acquisition; EKT: conceptualization, investigation, writing – review and editing, supervision, funding acquisition; WRF: investigation, writing – review and editing, funding acquisition; OCC: investigation, writing – review and editing; LA: investigation, writing – review and editing; SB: investigation, writing – review and

editing; AS: conceptualization, investigation, writing – review and editing, supervision, funding acquisition.

Data availability statement. – Chronology and proxy data presented in this paper are publicly available in both LiPD (McKay & Emile-Geay 2016) and text format at the National Centers for Environmental Information for Paleoclimatology. https://www.ncei.noaa.gov/access/paleo-search/study/39520. Water isotope data are freely available in the Water Isotopes Database: www.waterisotopes.org (Project ID 00400). [Correction added on 22 June 2024, after the first publication: In the Data Availability Statement, the URL for Paleoclimatology has been updated.]

References

Aichner, B., Herzschuh, U., Wilkes, H., Vieth, A. & Böhner, J. 2010: δD values of *n*-alkanes in Tibetan lake sediments and aquatic macrophytes – a surface sediment study and application to a 16 ka record from Lake Koucha. *Organic Geochemistry 41*, 779–790.

Allaart, L., Müller, J., Schomacker, A., Rydningen, T. A., Håkansson, L., Kjellman, S. E., Mollenhauer, G. & Forwick, M. 2020: Late Quaternary glacier and sea-ice history of northern Wijdefjorden, Svalbard. *Boreas 49*, 417–437.

Allaart, L., Schomacker, A., Larsen, N. K., Nørmark, E., Rydningen, T. A., Farnsworth, W. R., Retelle, M., Brynjólfsson, S., Forwick, M. & Kjellman, S. E. 2021: Glacial history of the Åsgardfonna Ice Cap, NE Spitsbergen, since the last glaciation. *Quaternary Science Reviews 251*, 106717, https://doi.org/10.1016/j.quascirev.2020.106717.

Anderson, L., Abbott, M. B., Finney, B. P. & Burns, S. J. 2007: Late Holocene moisture balance variability in the southwest Yukon Territory, Canada. *Quaternary Science Reviews 26*, 130–141.

Arppe, L., Kurki, E., Wooller, M. J., Luoto, T. P., Zajączkowski, M. & Ojala, A. E. 2017: A 5500-year oxygen isotope record of high arctic environmental change from southern Spitsbergen. *The Holocene 27*, 1948–1962.

Balascio, N. L., D'Andrea, W. J., Bradley, R. S. & Perren, B. B. 2013: Biogeochemical evidence for hydrologic changes during the Holocene in a lake sediment record from southeast Greenland. *The Holocene 23*, 1428–1439.

Balascio, N. L., D'Andrea, W. J., Gjerde, M. & Bakke, J. 2018: Hydroclimate variability of High Arctic Svalbard during the Holocene inferred from hydrogen isotopes of leaf waxes. *Quaternary Science Reviews 183*, 177–187.

Bartels, M., Titschack, J., Fahl, K., Stein, R. & Hebbeln, D. 2018: Wahlenbergfjord, eastern Svalbard: a glacier-surrounded fjord reflecting regional hydrographic variability during the Holocene? *Boreas 47*, 1003–1021.

Bartels, M., Titschack, J., Fahl, K., Stein, R., Seidenkrantz, M.-S., Hillaire-Marcel, C. & Hebbeln, D. 2017: Atlantic Water advection vs. glacier dynamics in northern Spitsbergen since early deglaciation. *Climate of the Past 13*, 1717–1749.

Berke, M. A., Sierra, A. C., Bush, R., Cheah, D. & O'Connor, K. 2019: Controls on leaf wax fractionation and δ^2H values in tundra vascular plants from western Greenland. *Geochimica et Cosmochimica Acta 244*, 565–583.

van der Bilt, W. G., Bakke, J., Vasskog, K., D'Andrea, W. J., Bradley, R. S. & Ólafsdóttir, S. 2015: Reconstruction of glacier variability from lake sediments reveals dynamic Holocene climate in Svalbard. *Quaternary Science Reviews 126*, 201–218.

van der Bilt, W. G., D'Andrea, W. J., Bakke, J., Balascio, N. L., Werner, J. P., Gjerde, M. & Bradley, R. S. 2018: Alkenone-based reconstructions reveal four-phase Holocene temperature evolution for high Arctic Svalbard. *Quaternary Science Reviews 183*, 204–213.

van der Bilt, W. G., D'Andrea, W. J., Werner, J. P. & Bakke, J. 2019: Early Holocene temperature oscillations exceed amplitude of observed and projected warming in Svalbard lakes. *Geophysical Research Letters 46*, 14732–14741.

Birks, H. H. 1991: Holocene vegetational history and climatic change in west Spitsbergen-plant macrofossils from Skardtjørna, an Arctic lake. *The Holocene 1*, 209–218.

Blaauw, M. & Christen, J. A. 2011: Flexible paleoclimate age-depth models using an autoregressive gamma process. *Bayesian Analysis 6*, 457–474.

Bonne, J. L., Meyer, H., Behrens, M., Boike, J., Kipfstuhl, S., Rabe, B., Schmidt, T., Schönicke, L., Steen-Larsen, H. C. & Werner, M. 2020: Moisture origin as a driver of temporal variabilities of the water vapour isotopic composition in the Lena River Delta, Siberia. *Atmospheric Chemistry and Physics 20*, 10493–10511.

Bowen, G. J. 2021: OIPC: The online isotopes in precipitation calculator, version 3.1. Available at: http://www.waterisotopes.org.

Bowen, G. J. & Revenaugh, J. 2003: Interpolating the isotopic composition of modern meteoric precipitation. *Water Resources Research 39*, 1299, https://doi.org/10.1029/2003WR002086.

Bowen, G. J., Wassenaar, L. I. & Hobson, K. A. 2005: Global application of stable hydrogen and oxygen isotopes to wildlife forensics. *Oecologia 143*, 337–348.

Broadman, E., Kaufman, D. S., Henderson, A. C., Malmierca-Vallet, I., Leng, M. J. & Lacey, J. H. 2020: Coupled impacts of sea ice variability and North Pacific atmospheric circulation on Holocene hydroclimate in Arctic Alaska. *Proceedings of the National Academy of Sciences 117*, 33034–33042.

Bush, R. T., Berke, M. A. & Jacobson, A. D. 2017: Plant water δD and δ^{18}O of tundra species from West Greenland. *Arctic, Antarctic, and Alpine Research 49*, 341–358.

Cluett, A. A. & Thomas, E. K. 2020: Resolving combined influences of inflow and evaporation on western Greenland lake water isotopes to inform paleoclimate inferences. *Journal of Paleolimnology 63*, 251–268.

Cluett, A., Thomas, E., Evans, S. & Keys, P. 2021: Seasonal variations in moisture origin explain spatial contrast in precipitation isotope seasonality on coastal western Greenland. *Journal of Geophysical Research: Atmospheres 126*, e2020JD033543, https://doi.org/10.1029/2020JD033543.

Cooper, L., Olsen, C., Solomon, D., Larsen, I., Cook, R. & Grebmeier, J. 1991: Stable isotopes of oxygen and natural and fallout radionuclides used for tracing runoff during snowmelt in an Arctic watershed. *Water Resources Research 27*, 2171–2179.

Corcoran, M. C., Thomas, E. K. & Morrill, C. 2021: Using a paired chironomid δ^{18}O and aquatic leaf wax δ^2H approach to reconstruct seasonality on western Greenland during the Holocene. *Paleoceanography and Paleoclimatology 36*, e2020PA004169, https://doi.org/10.1029/2020PA004169.

Cowling, O. C., Thomas, E. K., Svendsen, J. I., Mangerud, J., Haflidason, H., Regnéll, C. & Brendryen, J. 2021: Western Siberia experienced rapid shifts in moisture source and summer water balance during the last deglaciation and early Holocene. *Journal of Quaternary Science 37*, 790–804.

Craig, H. 1961: Isotopic variations in meteoric waters. *Science 133*, 1702–1703.

D'Andrea, W. J., Vaillencourt, D. A., Balascio, N. L., Werner, A., Roof, S. R., Retelle, M. & Bradley, R. S. 2012: Mild Little Ice Age and unprecedented recent warmth in an 1800 year lake sediment record from Svalbard. *Geology 40*, 1007–1010, https://doi.org/10.1130/G33365.1.

Daniels, W. C., Russell, J. M., Giblin, A. E., Welker, J. M., Klein, E. S. & Huang, Y. 2017: Hydrogen isotope fractionation in leaf waxes in the Alaskan Arctic tundra. *Geochimica et Cosmochimica Acta 213*, 216–236.

Daniels, W. C., Russell, J., Morrill, C., Longo, W., Giblin, A., Holland-Stergar, P., Welker, J., Wen, X., Hu, A. & Huang, Y. 2021: Lacustrine leaf wax hydrogen isotopes indicate strong regional climate feedbacks in Beringia since the last ice age. *Quaternary Science Reviews 269*, 107130, https://doi.org/10.1016/j.quascirev.2021.107130.

Dansgaard, W. 1964: Stable isotopes in precipitation. *Tellus 16*, 436–468.

Diefendorf, A. F. & Freimuth, E. J. 2017: Extracting the most from terrestrial plant-derived *n*-alkyl lipids and their carbon isotopes from the sedimentary record: a review. *Organic Geochemistry 103*, 1–21.

Dion-Kirschner, H., McFarlin, J. M., Masterson, A. L., Axford, Y. & Osburn, M. R. 2020: Modern constraints on the sources and climate signals recorded by sedimentary plant waxes in west Greenland. *Geochimica et Cosmochimica Acta 286*, 336–354.

Dufour, A., Zolina, O. & Gulev, S. K. 2016: Atmospheric moisture transport to the Arctic: assessment of reanalyses and analysis of transport components. *Journal of Climate 29*, 5061–5081.

Eckerstorfer, M. & Christiansen, H. H. 2011: The "High Arctic Maritime Snow Climate" in Central Svalbard. *Arctic, Antarctic, and Alpine Research 43*, 11–21.

Eidesen, P. B., Arnesen, G., Elven, R. & Søli, G. 2018: *Kartlegging av Ringhorndalen, Wijdefjorden: En Uutforsket Arktisk Oase*. 43 pp. The University Centre in Svalbard, The University of Oslo, Ecofact Nord AS. Available at: https://www.miljovernfondet.no/wp-content/uploads/2020/02/14-108-sluttrapport-ringhorndalen.pdf.

Farnsworth, W. R., Allaart, L., Ingólfsson, Ó., Alexanderson, H., Forwick, M., Noormets, R., Retelle, M. & Schomacker, A. 2020: Holocene glacial history of Svalbard: status, perspectives and challenges. *Earth-Science Reviews 208*, 103249, https://doi.org/10.1016/j.earscirev.2020.103249.

Farnsworth, W. R., Ingólfsson, Ó., Mannerfelt, E. S., Kalliokoski, M. H., GuÞmundsdóttir, E. R., Retelle, M., Allaart, L., Brynjólfsson, S., Furze, M. F., Hancock, H. J., Kjær, K. H., Pieńkowski, A. J. & Schomacker, A. 2022: Vedde Ash constrains Younger Dryas glacier re-advance and rapid glacio-isostatic rebound on Svalbard. *Quaternary Science Advances 5*, 100041, https://doi.org/10.1016/j.qsa.2021.100041.

Farnsworth, W. R., Ingólfsson, Ó., Retelle, M., Allaart, L., Håkansson, L. M. & Schomacker, A. 2018: Svalbard glaciers re-advanced during the Pleistocene–Holocene transition. *Boreas 47*, 1022–1032.

Ficken, K. J., Li, B., Swain, D. & Eglinton, G. 2000: An *n*-alkane proxy for the sedimentary input of submerged/floating freshwater aquatic macrophytes. *Organic Geochemistry 31*, 745–749.

Fjeldskaar, W., Bondevik, S. & Amantov, A. 2018: Glaciers on Svalbard survived the Holocene thermal optimum. *Quaternary Science Reviews 199*, 18–29.

Førland, E. J. & Hanssen-Bauer, I. 2003: Past and future climate variations in the Norwegian Arctic: overview and novel analyses. *Polar Research 22*, 113–124.

Førland, E. J., Isaksen, K., Lutz, J., Hanssen-Bauer, I., Schuler, T. V., Dobler, A., Gjelten, H. M. & Vikhamar-Schuler, D. 2020: Measured and modeled historical precipitation trends for Svalbard. *Journal of Hydrometeorology 21*, 1279–1296.

Forwick, M. & Vorren, T. O. 2009: Late Weichselian and Holocene sedimentary environments and ice rafting in Isfjorden, Spitsbergen. *Palaeogeography, Palaeoclimatology, Palaeoecology 280*, 258–274.

Freimuth, E. J., Diefendorf, A. F. & Lowell, T. V. 2017: Hydrogen isotopes of *n*-alkanes and *n*-alkanoic acids as tracers of precipitation in a temperate forest and implications for paleorecords. *Geochimica et Cosmochimica Acta 206*, 166–183.

Fritz, P. & Clark, I. D. 1997: *Environmental Isotopes in Hydrogeology*. 342 pp. CRC Press, Boca Raton.

Gjerde, M., Bakke, J., D'Andrea, W. J., Balascio, N. L., Bradley, R. S., Vasskog, K., Ólafsdóttir, S., Røthe, T. O., Perren, B. B. & Hormes, A. 2018: Holocene multi-proxy environmental reconstruction from lake Hakluytvatnet, Amsterdamøya Island, Svalbard (79.5°N). *Quaternary Science Reviews 183*, 164–176.

Gorbey, D. B., Thomas, E. K., Crump, S. E., Hollister, K. V., Raynolds, M. K., Raberg, J. H., de Wet, G., Sepúlveda, J. & Miller, G. H. 2021: Southern Baffin Island mean annual precipitation isotopes modulated by summer and autumn moisture source changes during the past 5800 years. *Journal of Quaternary Science 37*, 967–978.

Gorbey, D. B., Thomas, E. K., Sauer, P. E., Raynolds, M. K., Miller, G. H., Corcoran, M. C., Cowling, O. C., Crump, S. E., Lovell, K. & Raberg, J. H. 2022: Modern eastern Canadian Arctic Lake water isotopes exhibit latitudinal patterns in inflow seasonality and minimal evaporative enrichment. *Paleoceanography and Paleoclimatology 37*, e2021PA004384, https://doi.org/10.1029/2021PA004384.

Guo, C.-Q., Ochyra, R., Wu, P.-C., Seppelt, R. D., Yao, Y.-F., Bian, L.-G., Li, S.-P. & Li, C.-S. 2013: *Warnstorfia exannulata*, an aquatic moss in the Arctic: seasonal growth responses. *Climatic Change 119*, 407–419.

Hald, M., Andersson, C., Ebbesen, H., Jansen, E., Klitgaard-Kristensen, D., Risebrobakken, B., Salomonsen, G. R., Sarnthein, M., Sejrup, H. P. & Telford, R. J. 2007: Variations in temperature and extent of Atlantic Water in the northern North Atlantic during the Holocene. *Quaternary Science Reviews 26*, 3423–3440.

Hald, M., Ebbesen, H., Forwick, M., Godtliebsen, F., Khomenko, L., Korsun, S., Olsen, L. R. & Vorren, T. O. 2004: Holocene paleoceanography and glacial history of the West Spitsbergen area, Euro-Arctic margin. *Quaternary Science Reviews 23*, 2075–2088.

Hanssen-Bauer, I., Førland, E. J., Hisdal, H., Mayer, S., Sandø, A. B. & Sorteberg, A. 2019: *Climate in Svalbard 2100 – A Knowledge Base for Climate Adaptation*. 207 pp. Norwegian Centre for Climate Services (NCCS), NCCS report no. 1/2019. Available at: https://www.miljodirektoratet.no/globalassets/publikasjoner/M1242/M12 42.pdf.

Harrington, T. S., Zhu, J. & Skinner, C. B. 2021: Terrestrial sources of summer arctic moisture and the implication for arctic temperature patterns. *npj Climate and Atmospheric Science 4*, 25, https://doi.org/10.1038/s41612-021-00181-y.

Hisdal, V. 1998: *Svalbard: Nature and History*. 123 pp. *Polarhåndbok No. 12*. Norwegian Polar Institute, Tromsø.

Hollister, K. V., Thomas, E. K., Raynolds, M. K., Bültmann, H., Raberg, J. H., Miller, G. H. & Sepúlveda, J. 2022: Aquatic and terrestrial plant contributions to sedimentary plant waxes in a modern Arctic lake setting. *Journal of Geophysical Research: Biogeosciences 127*, e2022JG006903, https://doi.org/10.1029/2022JG006903.

Holm, T. M., Koinig, K. A., Andersen, T., Donali, E., Hormes, A., Klaveness, D. & Psenner, R. 2012: Rapid physicochemical changes in the high Arctic Lake Kongressvatn caused by recent climate change. *Aquatic Sciences 74*, 385–395.

Huang, Y., Shuman, B., Wang, Y. & Webb, T. 2004: Hydrogen isotope ratios of individual lipids in lake sediments as novel tracers of climatic and environmental change: a surface sediment test. *Journal of Paleolimnology 31*, 363–375.

Humlum, O. 2002: Modelling late 20th-century precipitation in Nordenskiöld Land, Svalbard, by geomorphic means. *Norsk Geografisk Tidsskrift-Norwegian Journal of Geography 56*, 96–103.

Humlum, O. 2005: Holocene permafrost aggradation in Svalbard. *Geological Society, London, Special Publications 242*, 119–129.

Husum, K. & Hald, M. 2012: Arctic planktic foraminiferal assemblages: implications for subsurface temperature reconstructions. *Marine Micropaleontology 96*, 38–47.

IAEA/WMO 2019: Global network of isotopes in precipitation. The GNIP database. Available at: https://nucleus.iaea.org/wiser.

Icelandic Met Office 2024: Monthly averages for station 178 – Stykkishólmur. Available at: https://www.vedur.is/Medaltalstoflur-txt/Stod_178_Stykkisholmur.ManMedal.txt.

Jakobsson, M., Mayer, L., Coakley, B., Dowdeswell, J. A., Forbes, S., Fridman, B., Hodnesdal, H., Noormets, R., Pedersen, R. & Rebesco, M. 2012: The international bathymetric chart of the Arctic Ocean (IBCAO) version 3.0. *Geophysical Research Letters 39*, L12609, https://doi.org/10.1029/2012GL052219.

Jennings, A. E., Andrews, J. A., Pearce, C., Wilson, L. & Ólafsdóttir, S. 2015: Reconstruction of Sea Surface Temperatures for sediment core MD99-2256 [data set]. *PANGAEA*, https://doi.org/10.1594/PANGAEA.864059. Supplement to: Jennings, A. E. *et al.* 2015: Detrital carbonate peaks on the Labrador shelf, a 13–7 ka template for freshwater forcing from the Hudson Strait outlet of the Laurentide Ice Sheet into the subpolar gyre. *Quaternary Science Reviews 107*, 62–80.

Jonsson, C. E., Leng, M. J., Rosqvist, G. C., Seibert, J. & Arrowsmith, C. 2009: Stable oxygen and hydrogen isotopes in sub-Arctic lake waters from northern Sweden. *Journal of Hydrology 376*, 143–151.

Kahmen, A., Schefuß, E. & Sachse, D. 2013: Leaf water deuterium enrichment shapes leaf wax *n*-alkane δD values of angiosperm plants I: experimental evidence and mechanistic insights. *Geochimica et Cosmochimica Acta 111*, 39–49.

Karlsen, S. R., Elvebakk, A., Høgda, K. A. & Grydeland, T. 2014: Spatial and temporal variability in the onset of the growing season on Svalbard, Arctic Norway–measured by MODIS-NDVI satellite data. *Remote Sensing 6*, 8088–8106.

Katrantsiotis, C., Norström, E., Smittenberg, R. H., Salonen, J. S., Plikk, A. & Helmens, K. 2021: Seasonal variability in temperature trends and atmospheric circulation systems during the Eemian (Last Interglacial) based on *n*-alkanes hydrogen isotopes from Northern Finland. *Quaternary Science Reviews 273*, 107250, https://doi.org/10.1016/j.quascirev.2021.107250.

Keisling, B. A., Castañeda, I. S. & Brigham-Grette, J. 2017: Hydrological and temperature change in Arctic Siberia during the intensification of Northern Hemisphere Glaciation. *Earth and Planetary Science Letters 457*, 136–148.

Kjellman, S. E. 2022: *Holocene precipitation seasonality on Svalbard and in Northern Fennoscandia reconstructed using organic geochemical and stable isotope proxies.* Doctoral thesis, UiT The Arctic University of Norway, 188 pp. Available at: https://hdl.handle.net/10037/26641.

Kjellman, S. E., Schomacker, A., Thomas, E. K., Håkansson, L., Duboscq, S., Cluett, A. A., Farnsworth, W. R., Allaart, L., Cowling, O. C. & McKay, N. P. 2020: Holocene precipitation seasonality in northern Svalbard: influence of sea ice and regional ocean surface conditions. *Quaternary Science Reviews 240*, 106388, https://doi.org/10.1016/j.quascirev.2020.106388.

Kjellman, S. E., Thomas, E. K. & Schomacker, A. 2022: Arctic and sub-Arctic lake water δ^2H and $\delta^{18}O$ along a coastal-inland transect: implications for interpreting water isotope proxy records. *Journal of Hydrology 607*, 127556, https://doi.org/10.1016/j.jhydrol.2022.127556.

Konecky, B. L., McKay, N. P., Comas-Bru, L., Dassié, E. P., DeLong, K. L., Falster, G. M., Fischer, M. J., Jones, M. D., Jonkers, L. & Kaufman, D. S. 2020: The Iso2k database: a global compilation of paleo-$\delta^{18}O$ and δ^2H records to aid understanding of Common Era climate. *Earth System Science Data 12*, 2261–2288.

Köseoğlu, D., Belt, S. T., Smik, L., Yao, H., Panieri, G. & Knies, J. 2018: Complementary biomarker-based methods for characterising Arctic sea ice conditions: a case study comparison between multivariate analysis and the PIP25 index. *Geochimica et Cosmochimica Acta 222*, 406–420.

Lamhonwah, D., Lafrenière, M. J., Lamoureux, S. F. & Wolfe, B. B. 2017: Evaluating the hydrological and hydrochemical responses of a High Arctic catchment during an exceptionally warm summer. *Hydrological Processes 31*, 2296–2313.

Lapointe, F., Retelle, M., Bradley, R., Farnsworth, W. R., Støren, E., Cook, T. & Rosario, J. 2023: Multi-proxy evidence of unprecedented hydroclimatic change in a High Arctic proglacial lake: Linnévatnet, Svalbard. *Arctic, Antarctic, and Alpine Research 55*, 2223403, https://doi.org/10.1080/15230430.2023.2223403.

Laskar, J., Robutel, P., Joutel, F., Gastineau, M., Correia, A. & Levrard, B. 2004: A long-term numerical solution for the insolation quantities of the Earth. *Astronomy & Astrophysics 428*, 261–285.

Leroy-Dos Santos, C., Masson-Delmotte, V., Casado, M., Fourré, E., Steen-Larsen, H. C., Maturilli, M., Orsi, A., Berchet, A., Cattani, O., Minster, B., Gherardi, J. & Landais, A. 2020: A 4.5 year-long record of Svalbard water vapor isotopic composition documents winter air mass origin. *Journal of Geophysical Research: Atmospheres 125*, e2020JD032681, https://doi.org/10.1029/2020JD032681.

Linderholm, H. W., Nicolle, M., Francus, P., Gajewski, K., Helama, S., Korhola, A., Solomina, O., Yu, Z., Zhang, P. & D'Andrea, W. J. 2018: Arctic hydroclimate variability during the last 2000 years. *Climate of the Past 14*, 473–514.

Lønne, I. 2005: Faint traces of high Arctic glaciations: an early Holocene ice-front fluctuation in Bolterdalen, Svalbard. *Boreas 34*, 308–323.

MacDonald, L. A., Wolfe, B. B., Turner, K. W., Anderson, L., Arp, C. D., Birks, S. J., Bouchard, F., Edwards, T. W., Farquharson, N. & Hall, R. I. 2017: A synthesis of thermokarst lake water balance in high-latitude regions of North America from isotope tracers. *Arctic Science 3*, 118–149.

Mangerud, J. & Svendsen, J. I. 2018: The Holocene Thermal Maximum around Svalbard, Arctic North Atlantic; molluscs show early and exceptional warmth. *The Holocene 28*, 65–83.

Masson-Delmotte, V., Landais, A., Stievenard, M., Cattani, O., Falourd, S., Jouzel, J., Johnsen, S. J., Dahl-Jensen, D., Sveinbjörnsdóttir, Á. & White, J. 2005: Holocene climatic changes in Greenland: different deuterium excess signals at Greenland Ice Core Project (GRIP) and NorthGRIP. *Journal of Geophysical Research: Atmospheres 110*, D14, https://doi.org/10.1029/2004JD005575.

McFarlin, J. M., Axford, Y., Kusch, S., Masterson, A. L., Lasher, G. E. & Osburn, M. R. 2023: Aquatic plant wax hydrogen and carbon isotopes in Greenland lakes record shifts in methane cycling during past Holocene warming. *Science Advances 9*, eadh9704, https://doi.org/10.1126/sciadv.adh9704.

McFarlin, J. M., Axford, Y., Masterson, A. L. & Osburn, M. R. 2019: Calibration of modern sedimentary δ^2H plant wax-water relationships in Greenland lakes. *Quaternary Science Reviews 225*, 105978, https://doi.org/10.1016/j.quascirev.2019.105978.

McKay, N. & Emile-Geay, J. 2016: Technical note: The Linked Paleo Data framework–a common tongue for paleoclimatology. *Climate of the Past 12*, 1093–1100.

McKay, N. P., Emile-Geay, J. & Khider, D. 2021: geoChronR–an R package to model, analyze, and visualize age-uncertain data. *Geochronology 3*, 149–169.

MET Norway 2021: seKlima. Available at: https://klimaservicesenter.no/observations/.

Miller, G. H., Landvik, J. Y., Lehman, S. J. & Southon, J. R. 2017: Episodic Neoglacial snowline descent and glacier expansion on Svalbard reconstructed from the ^{14}C ages of ice-entombed plants. *Quaternary Science Reviews 155*, 67–78.

Müller, M., Kelder, T. & Palerme, C. 2022: Decline of sea-ice in the Greenland Sea intensifies extreme precipitation over Svalbard. *Weather and Climate Extremes 36*, 100437, https://doi.org/10.1016/j.wace.2022.100437.

Müller, J., Werner, K., Stein, R., Fahl, K., Moros, M. & Jansen, E. 2012: Holocene cooling culminates in sea ice oscillations in Fram Strait. *Quaternary Science Reviews 47*, 1–14.

National Snow and Ice Data Center 2019: SOTC: Sea ice. Available at: http://nsidc.org/cryosphere/sotc/sea_ice.html.

Nordli, P. Ä., Hanssen-Bauer, I. & Førland, E. 1996: *Homogeneity Analyses of Temperature and Precipitation Series from Svalbard and Jan Mayen*. 41 pp. *DNMI Report no. 16/96 KLIMA*. Norges Meteorologiske Institutt, Oslo.

Norwegian Polar Institute 2014: Terrengmodell Svalbard (S0 Terrengmodell). Available at: https://doi.org/10.21334/npolar.2014.dce53a47.

Nusbaumer, J., Alexander, P. M., LeGrande, A. N. & Tedesco, M. 2019: Spatial shift of Greenland moisture sources related to enhanced Arctic warming. *Geophysical Research Letters 46*, 14723–14731.

ORNL DAAC 2018: *MODIS and VIIRS Land Products Global Subsetting and Visualization Tool*. ORNL DAAC, Oak Ridge, Available at: https://doi.org/10.3334/ORNLDAAC/1379.

Paillard, D., Labeyrie, L. & Yiou, P. 1996: AnalySeries 1.0: a Macintosh software for the analysis of geophysical time-series. *Eos 77*, 379, https://doi.org/10.1029/96EO00259.

Pieńkowski, A. J., Husum, K., Belt, S. T., Ninnemann, U., Köseoğlu, D., Divine, D. V., Smik, L., Knies, J., Hogan, K. & Noormets, R. 2021: Seasonal sea ice persisted through the Holocene Thermal Maximum at 80°N. *Communications Earth & Environment 2*, 1–10.

R Core Team 2021: *R: A Language and Environment for Statistical Computing*. R Foundation for Statistical Computing, Vienna. Available at: https://www.R-project.org/.

Rach, O., Kahmen, A., Brauer, A. & Sachse, D. 2017: A dual-biomarker approach for quantification of changes in relative humidity from sedimentary lipid D/ H ratios. *Climate of the Past 13*, 741–757.

Reimer, P. J., Austin, W. E., Bard, E., Bayliss, A., Blackwell, P. G., Ramsey, C. B., Butzin, M., Cheng, H., Edwards, R. L. & Friedrich, M. 2020: The IntCal20 Northern Hemisphere radiocarbon age calibration curve (0–55 cal kBP). *Radiocarbon 62*, 725–757.

Riis, T., Christoffersen, K. S. & Baattrup-Pedersen, A. 2014: Effects of warming on annual production and nutrient-use efficiency of aquatic mosses in a high Arctic lake. *Freshwater Biology 59*, 1622–1632.

Røthe, T. O., Bakke, J., Støren, E. W. & Bradley, R. S. 2018: Reconstructing Holocene glacier and climate fluctuations from lake sediments in Vårfluesjøen, northern Spitsbergen. *Frontiers in Earth Science 6*, 91, doi: 10.3389/feart.2018.00091.

Røthe, T. O., Bakke, J., Vasskog, K., Gjerde, M., D'Andrea, W. J. & Bradley, R. S. 2015: Arctic Holocene glacier fluctuations reconstructed from lake sediments at Mitrahalvøya, Spitsbergen. *Quaternary Science Reviews 109*, 111–125.

Rozanski, K., Araguás-Araguás, L. & Gonfiantini, R. 1993: Isotopic patterns in modern global precipitation. *In* Swart, P. K., Lohmann, K. C., Mckenzie, J. & Savin, S. (eds.): *Climate Change in Continental Isotopic Records. Geophysical Monograph Series*, vol. *78*, 1–36. American Geophysical Union, Washington.

Sachse, D., Billault, I., Bowen, G. J., Chikaraishi, Y., Dawson, T. E., Feakins, S. J., Freeman, K. H., Magill, C. R., McInerney, F. A., van der Meer, M. T. J., Polissar, P., Robins, R. J., Sachs, J. P., Schmidt, H.-L., Sessions, A. L., White, J. W. C., West, J. B. & Kahmen, A. 2012: Molecular paleohydrology: interpreting the hydrogen-isotopic composition of lipid biomarkers from photosynthesizing organisms. *Annual Review of Earth and Planetary Sciences 40*, 221–249.

Sachse, D., Radke, J. & Gleixner, G. 2004: Hydrogen isotope ratios of recent lacustrine sedimentary n-alkanes record modern climate variability. *Geochimica et Cosmochimica Acta 68*, 4877–4889.

Sand, K., Winther, J.-G., Maréchal, D., Bruland, O. & Melvold, K. 2003: Regional variations of snow accumulation on Spitsbergen, Svalbard, 1997–99. *Hydrology Research 34*, 17–32.

Sarnthein, M., Van Kreveld, S., Erlenkeuser, H., Grootes, P. M., Kucera, M., Pflaumann, U. & Schulz, M. 2003: Centennial-to-millennial-scale periodicities of Holocene climate and sediment injections off the western Barents shelf, 75°N. *Boreas 32*, 447–461.

Schomacker, A., Farnsworth, W. R., Ingólfsson, Ó., Allaart, L., Håkansson, L., Retelle, M., Siggaard-Andersen, M.-L., Korsgaard, N. J., Rouillard, A. & Kjellman, S. E. 2019: Postglacial relative sea level change and glacier activity in the early and late Holocene: Wahlenbergfjorden, Nordaustlandet, Svalbard. *Scientific Reports 9*, 6799, https://doi.org/10.1038/s41598-019-43342-z.

Serreze, M. C., Barrett, A. P., Slater, A. G., Steele, M., Zhang, J. & Trenberth, K. E. 2007: The large-scale energy budget of the Arctic. *Journal of Geophysical Research: Atmospheres 112*, D11, https://doi.org/10.1029/2006JD008230.

Sessions, A. L., Burgoyne, T. W., Schimmelmann, A. & Hayes, J. M. 1999: Fractionation of hydrogen isotopes in lipid biosynthesis. *Organic Geochemistry 30*, 1193–1200.

Shanahan, T. M., Hughen, K. A., Ampel, L., Sauer, P. E. & Fornace, K. 2013: Environmental controls on the ^{2}H/^{1}H values of terrestrial leaf waxes in the eastern Canadian Arctic. *Geochimica et Cosmochimica Acta 119*, 286–301.

Singh, H. K., Bitz, C. M., Donohoe, A. & Rasch, P. J. 2017: A source–receptor perspective on the polar hydrologic cycle: sources, seasonality, and Arctic-Antarctic parity in the hydrologic cycle response to CO_2 doubling. *Journal of Climate 30*, 9999–10017.

Skagseth, Ä., Furevik, T., Ingvaldsen, R., Loeng, H., Mork, K. A., Orvik, K. A. & Ozhigin, V. 2008: Volume and heat transports to the Arctic Ocean via the Norwegian and Barents Seas. *In* Dickson, R. R., Meincke, J. & Rhines, P. (eds.): *Arctic–Subarctic Ocean Fluxes*, 45–64. Springer, Dordrecht.

Steen-Larsen, H. C., Sveinbjörnsdottir, A. E., Jonsson, T., Ritter, F., Bonne, J. L., Masson-Delmotte, V., Sodemann, H., Blunier, T., Dahl-Jensen, D. & Vinther, B. M. 2015: Moisture sources and synoptic to seasonal variability of North Atlantic water vapor isotopic composition. *Journal of Geophysical Research: Atmospheres 120*, 5757–5774.

Sugimoto, A., Naito, D., Yanagisawa, N., Ichiyanagi, K., Kurita, N., Kubota, J., Kotake, T., Ohata, T., Maximov, T. C. & Fedorov, A. N. 2003: Characteristics of soil moisture in permafrost observed in East Siberian taiga with stable isotopes of water. *Hydrological Processes 17*, 1073–1092.

Svendsen, J. I. & Mangerud, J. 1997: Holocene glacial and climatic variations on Spitsbergen, Svalbard. *The Holocene 7*, 45–57.

Thomas, E. K., Briner, J. P., Ryan-Henry, J. J. & Huang, Y. 2016: A major increase in winter snowfall during the middle Holocene on western Greenland caused by reduced sea ice in Baffin Bay and the Labrador Sea. *Geophysical Research Letters 43*, 5302–5308.

Thomas, E. K., Castañeda, I. S., McKay, N. P., Briner, J. P., Salacup, J. M., Nguyen, K. Q. & Schweinsberg, A. D. 2018: A wetter Arctic coincident with hemispheric warming 8000 years ago. *Geophysical Research Letters 45*, 10637–10647.

Thomas, E. K., Cluett, A. A., Erb, M. P., McKay, N. P., Briner, J. P., Castañeda, I. S., Corcoran, M. C., Cowling, O. C., Gorbey, D. B., Lindberg, K. R., Prince, K. K. & Salacup, J. 2023: Early Holocene Laurentide Ice Sheet retreat influenced summer atmospheric circulation in Baffin Bay. *Geophysical Research Letters 50*, e2023GL103428, doi: 10.1029/2023GL103428.

Thomas, E. K., Hollister, K. V., Cluett, A. A., Corcoran, M. C. & Briner, J. P. 2020: Reconstructing Arctic precipitation seasonality using aquatic leaf wax δ^2H in lakes with contrasting residence times. *Paleoceanography and Paleoclimatology 35*, e2020PA003886, doi: 10.1029/2020PA003886.

Thomas, E. K., McGrane, S., Briner, J. P. & Huang, Y. 2012: Leaf wax δ^2H and varve-thickness climate proxies from proglacial lake sediments, Baffin Island, Arctic Canada. *Journal of Paleolimnology 48*, 193–207.

Throckmorton, H. M., Newman, B. D., Heikoop, J. M., Perkins, G. B., Feng, X., Graham, D. E., O'Malley, D., Vesselinov, V. V., Young, J. & Wullschleger, S. D. 2016: Active layer hydrology in an arctic tundra ecosystem: quantifying water sources and cycling using water stable isotopes. *Hydrological Processes 30*, 4972–4986.

Tuttle, S. E., Roof, S. R., Retelle, M. J., Werner, A., Gunn, G. E. & Bunting, E. L. 2022: Evaluation of satellite-derived estimates of Lake Ice Cover Timing on Linnévatnet, Kapp Linné, Svalbard using in-situ data. *Remote Sensing 14*, 1311, https://doi.org/10.3390/rs14061311.

Vázquez, M., Nieto, R., Drumond, A. & Gimeno, L. 2016: Moisture transport into the Arctic: source-receptor relationships and the roles of atmospheric circulation and evaporation. *Journal of Geophysical Research: Atmospheres 121*, 13493–13509.

Vikhamar-Schuler, D., Førland, E. J., Lutz, J. & Gjelten, H. M. 2019: *Evaluation of Downscaled Reanalysis and Observations for Svalbard – Background Report for Climate in Svalbard 2100. NCCS report no. 4/2019*. Norwegian Centre for Climate Services (NCCS).

Voldstad, L. H., Alsos, I. G., Farnsworth, W. R., Heintzman, P. D., Håkansson, L., Kjellman, S. E., Rouillard, A., Schomacker, A. & Eidesen, P. B. 2020: A complete Holocene lake sediment ancient DNA record reveals long-standing high Arctic plant diversity hotspot in northern Svalbard. *Quaternary Science Reviews 234*, 106207, https://doi.org/10.1016/j.quascirev.2020.106207.

Walczowski, W. & Piechura, J. 2011: Influence of the West Spitsbergen Current on the local climate. *International Journal of Climatology 31*, 1088–1093.

Werner, A. 1993: Holocene moraine chronology, Spitsbergen, Svalbard: lichenometric evidence for multiple Neoglacial advances in the Arctic. *The Holocene 3*, 128–137.

Werner, K., Müller, J., Husum, K., Spielhagen, R. F., Kandiano, E. S. & Polyak, L. 2016: Holocene sea subsurface and surface water masses in the Fram Strait–Comparisons of temperature and sea-ice reconstructions. *Quaternary Science Reviews 147*, 194–209.

Werner, K., Spielhagen, R. F., Bauch, D., Hass, H. C. & Kandiano, E. 2013: Atlantic Water advection versus sea-ice advances in the eastern Fram Strait during the last 9 ka: multiproxy evidence for a two-phase Holocene. *Paleoceanography 28*, 283–295.

Wickström, S., Jonassen, M. O., Vihma, T. & Uotila, P. 2020: Trends in cyclones in the high-latitude North Atlantic during 1979–2016. *Quarterly Journal of the Royal Meteorological Society 146*, 762–779.

Wilkie, K. M. K. 2012: Compound-Specific Hydrogen Isotopes of Lipid Biomarkers in Lake El'gygytgyn, NE Russia. *Electronic Doctoral Dissertations for UMass Amherst. Paper AAI3518289*. Available at: https://scholarworks.umass.edu/open_access_dissertations/561.

Wilkie, K. M. K., Chapligin, B., Meyer, H., Burns, S., Petsch, S. & Brigham-Grette, J. 2013: Modern isotope hydrology and controls on δD of plant leaf waxes at Lake El'gygytgyn, NE Russia. *Climate of the Past 9*, 335–352.

Woo, M. K., Kane, D. L., Carey, S. K. & Yang, D. 2008: Progress in permafrost hydrology in the new millennium. *Permafrost and Periglacial Processes 19*, 237–254.

Supporting Information

Additional Supporting Information to this article is available at http://www.boreas.dk.

Data S1. Study site descriptions.

Data S2. Rayleigh distillation simulations.

Data S3. Leaf wax concentrations and chain-length distributions.

Data S4. References to Supporting Information.

Fig. S1. Core overviews for Heftyevatnet (A) (Farnsworth *et al.* 2022), Jodavannet (B) (Voldstad *et al.* 2020), Austre Nevlingen (C) (Kjellman *et al.* 2020) and Kløverbladvatna (D) (Schomacker *et al.* 2019), including core photograph, X-ray image, lithological units, depths for leaf wax samples and calibrated radiocarbon ages and one tephra age (Table S3). For details on the correlation between the cores, see Fig. S2. The uppermost 2 m of the Heftyevatnet record were not described previously but constitute a continuation of unit 2 of Farnsworth *et al.* (2022).

Fig. S2. Stratigraphical correlation of lake sediment cores from Heftyevatnet (A), Jodavannet (B), Austre Nevlingen (C) and Kløverbladvatna (D), based on X-ray fluorescence (XRF) data and visual similarities in lithology, guided by radiocarbon age constraints. Overlapping cores were aligned in AnalySeries (v. 2.0.8; Paillard *et al.* 1996), and tie-points in the elemental data were used to construct a composite depth scale. Several elemental ratios and titanium normalized against the incoherent and coherent scatter (Ti/(inc+coh)) were used to correlate each set of cores, with a selection of them displayed in the figure. Depths refer to original core depths.

Fig. S3. Bayesian age-depth models for composite records from Heftyevatnet (A), Jodavannet (B), Austre Nevlingen (C) and Kløverbladvatna (D), generated using Bacon (Blaauw & Christen 2011) and the IntCal20 calibration curve (Reimer *et al.* 2020) within the geoChronR package (McKay *et al.* 2021). Calibrated radiocarbon dates are shown in black for surface cores and grey for piston cores. Details on each radiocarbon age are given in Table S3, and the lithological units displayed to the right are described in Fig. S1.

Fig. S4. Selected lake sediment proxies from Heftyevatnet. A. Leaf wax δ^2H. B. Leaf wax concentration. Values are cut off at 200 μg g^{-1} dry sediment (one sample at *c.* 9000 cal. a BP had higher values for three chain lengths: C_{24} = 472 μg g^{-1}; C_{26} =1044 μg g^{-1}; C_{28} = 335 μg g^{-1} dry sediment). C. Relative abundance (bars) and average chain length (ACL; line) distribution for even-chain C_{22} to C_{30} *n*-alkanoic acids. D. Calculated isotope difference between δ^2H_{precip} and δ^2H_{lake} ($\varepsilon_{precip-lake}$). E. Loss on ignition (LOI). Bold line: measured values plotted on the median age of each sample; fine line: median value of all age model iterations; light and dark shading: 1 and 2 σ age model uncertainty, respectively. For simplicity, age uncertainty shading is only shown on the C_{22} and C_{28} time series in A and excluded in B and C. Ca/Fe ratio (F) and Ti normalized by the incoherent and coherent signal Ti/(inc+coh) (G) presented for cores HBS1, HVP1 and HVP3 separately. The XRF data are plotted as raw data and with a 49-point running average. H. Simplified lithology. For details, see Fig. S1.

Fig. S5. Selected lake sediment proxies from Jodavannet. A. Leaf wax δ^2H. B. Leaf wax concentration. C. Relative abundance (bars) and average chain length (ACL; line) distribution for even-chain C_{22} to C_{30} *n*-alkanoic acids. D. Loss on ignition (LOI). Lines and shading are shown as in Fig. S4. Ca/Fe ratio (E) and Ti normalized by the incoherent and coherent signal Ti/(inc+coh) (F) presented for cores JVS1 and JVP1 separately. The XRF data are plotted as raw data and with a 49-point running average. G. Simplified lithology. For details, see Fig. S1.

Fig. S6. Selected lake sediment proxies from Austre Nevlingen. A. Leaf wax δ^2H. B. Leaf wax concentration. C. Relative abundance (bars) and average chain length (ACL; line) distribution for even-chain C_{22} to C_{30} *n*-alkanoic acids. D. Loss on ignition (LOI). Lines and shading are shown as in Fig. S4. Ca/Fe ratio (E) and Ti normalized by the incoherent and coherent signal Ti/(inc+coh) (F) presented for cores ANS1 and ANP3 separately. The XRF data are plotted as raw data and with a 49-point running average. G. Simplified lithology. For details, see Fig. S1.

Fig. S7. Selected lake sediment proxies from Kløverbladvatna. A. Leaf wax δ^2H. B. Leaf wax concentration. C. Relative abundance (bars) and average chain length (ACL; line) distribution for even-chain C_{22} to C_{30} *n*-alkanoic acids. D. Loss on ignition (LOI). Lines and shading are shown as in Fig. S4. Ca/Fe ratio (E) and Ti normalized by the incoherent and coherent signal Ti/(inc+coh) (F) presented for cores KLÄVS2 and KLÄVP2 separately. The XRF data are plotted as raw data and with a 49-point running average. G. Simplified lithology. For details, see Fig. S1.

Table S1. Calculations of seasonal runoff and residence times for Heftyevatnet, Jodavannet, Austre Nevlingen, and Kløverbladvatna, Svalbard.

Table S2. Parameters used in model runs for the Rayleigh distillation simulations. For locations, see Fig. 4.

Table S3. Radiocarbon ages from lake sediment cores from Svalbard. Calibrated ages are median ages within the 2σ age ranges. The samples Ua-64 589, LuS 14022, LuS 14023, LuS 14024, Ua-63429, LuS 14025 and LuS 17223 from Heftyevatnet and Ua-55367, Ua-55368 and

Ua-55369 from Jodavannet are new to this study. Other ages from Heftyevatnet and Jodavannet are published in Farnsworth *et al*. (2022) and Voldstad *et al*. (2020). Ages from Austre Nevlingen are published in Kjellman *et al*. (2020), and Kløverbladvatna in Schomacker *et al*. (2019).

Table S4. H_3^+ factors, determined at the beginning of each sequence.

Table S5. Interpretative framework for leaf wax-derived δ^2H values from Svalbard lakes investigated in this study. When deciding on the interpretation, we weight the lake water isotope measurements more heavily than the residence time calculations, since the lake water values are actual observations, and the residence time calculations are best estimates.